

29 ¹²Institute of Marine Research (IIM-CSIC), Rúa de Eduardo Cabello 6, Vigo 36208,
30 Pontevedra, Spain

31 ¹³Department of Marine Ecology. Center for Advanced Studies of Blanes (CEAB-CSIC),
32 Acceso Cala St. Francesc 14, Blanes 17300, Girona, Spain

33 ¹⁴Department of Marine Science, University of Southern Mississippi, Stennis Space Center, MS
34 39529, USA

35 ¹⁵Second Institute of Oceanography, Ministry of Natural Resources, P. R. China

36 ¹⁶IFREMER, Centre de Brest, Technopôle Brest Iroise, Plouzané, France

37 Correspondance: Paul Tréguer (paul.treguer@univ-brest.fr) and Jill Sutton ([jill.sutton@univ-](mailto:jill.sutton@univ-brest.fr)
38 [brest.fr](mailto:jill.sutton@univ-brest.fr))

39

40 **Abstract**

41 The element silicon (Si) is required for the growth of silicified organisms in marine
42 environments, such as diatoms. These organisms consume vast amounts of Si together with N,
43 P, and C, connecting the biogeochemical cycles of these elements. Thus, understanding the Si
44 cycle in the ocean is critical for understanding wider issues such as carbon sequestration by the
45 ocean's biological pump. In this review, we show that recent advances in process studies
46 indicate that total Si inputs and outputs, to and from the world ocean, are 57 % and 37 % higher,
47 respectively, than previous estimates. We also update the total ocean silicic acid inventory
48 value, which is about 24% higher than previously estimated. These changes are significant,
49 modifying factors such as the geochemical residence time of Si, which is now about 8,000
50 years, two times faster than previously assumed. In addition, we present an updated value of
51 the global annual pelagic biogenic silica production (255 Tmol-Si yr⁻¹) based on new data from
52 49 field studies and 18 model outputs, and provide a first estimate of the global annual benthic
53 biogenic silica production due to sponges (6 Tmol-Si yr⁻¹). Given these important
54 modifications, we hypothesize that the modern ocean Si cycle is at approximately steady state
55 with inputs = 14.8 (±2.6) Tmole-Si yr⁻¹ and outputs = 15.6 (±2.4) Tmole-Si yr⁻¹. Potential
56 impacts of global change on the marine Si cycle are discussed.

57

58 **1. Introduction**

59 Silicon, the seventh-most abundant element in the universe, is the second most abundant
60 element in the Earth's crust. The weathering of the Earth's crust by CO₂-rich rain water, a key
61 process in the control of atmospheric CO₂ (Berner et al., 1983; Wollast & Mackenzie, 1989),
62 results in the generation of silicic acid (dSi; Si(OH)₄) in aqueous environments. Silicifiers are
63 among the most important aquatic organisms, and include micro-organisms (e.g. diatoms,
64 rhizarians, silicoflagellates, several species of choanoflagellates), and macro-organisms (e.g.
65 siliceous sponges). Silicifiers use dSi to precipitate biogenic silica (bSi; SiO₂) as internal
66 (Moriceau et al., 2019) and/or external (Maldonado et al., 2019) structures. Phototrophic
67 silicifiers, such as diatoms, globally consume vast amounts of Si concomitantly with nitrogen
68 (N), phosphorous (P) and inorganic carbon (C), connecting the biogeochemistry of these
69 elements and contributing to the sequestration of atmospheric CO₂ in the ocean (Tréguer &
70 Pondaven, 2000). Heterotrophic organisms like rhizarians, choanoflagellates and sponges
71 produce bSi independently of the photoautotrophic processing of C and N, and bSi (Maldonado
72 et al., 2012, 2019).

Supprimé:

Supprimé: we

Supprimé: address the steady state hypothesis of the Si cycle for past and modern oceans, and propose a possible steady state scenario for the global ocean (inputs = outputs = 15.6 Tmol-Si yr⁻¹) and boundary exchange zone. Case studies for future programs are highlighted and p

Mis en forme : Non Surlignage

Mis en forme : Non Surlignage

Supprimé: that has been named "dark silica"

81 Understanding the Si cycle is critical for understanding the functioning of marine food webs,
82 biogeochemical cycles, and the biological carbon pump. Herein, we review recent advances in
83 field observations and modelling that have changed our understanding of the global Si cycle
84 and provide an update of four of the six net annual input fluxes and of all the output fluxes
85 previously estimated by Tréguer & De La Rocha (2013). Taking into account numerous field
86 studies in different marine provinces and model outputs, we re-estimate the Si production
87 (Nelson et al., 1995), review the potential contribution of rhizarians (Llopis Monferrer et al.,
88 2020) and picocyanobacteria (Ohnemus et al., 2016), and give an estimate of the total bSi
89 production by siliceous sponges using recently published data on sponge bSi in marine
90 sediments (Maldonado et al., 2019). We discuss the question of the balance/imbalance of the
91 marine Si biogeochemical cycle at different time scales, and we hypothesize that the modern
92 ocean Si cycle is potentially at steady state with inputs = 14.8 (± 2.6) Tmole-Si yr⁻¹
93 approximately balancing outputs = 15.6 (± 2.4) Tmole-Si yr⁻¹ (Fig. 1). Finally, we address the
94 question of the potential impact of anthropogenic activities on the global Si cycle and suggest
95 guidelines for future research endeavours.

Supprimé: reference value of

Mis en forme : Non Surlignage

Mis en forme : Non Surlignage

Mis en forme : Non Surlignage

Mis en forme : Non Surlignage

Supprimé: propose a possible steady state scenario for the modern ocean, with inputs balancing outputs at 15.6 Tmol yr⁻¹

97 2. Advances in input fluxes

98 Silicic acid is delivered to the ocean through six pathways as illustrated in Fig. 1, which all
99 ultimately derive from the weathering of the Earth's crust (Tréguer & De La Rocha, 2013). All
100 fluxes are given with an error of one standard deviation.

Mis en forme : Non Surlignage

101 2.1 Riverine (F_R) and Aeolian (F_A) contributions

102 The best estimate for the riverine input (F_R) of dSi, based on data representing 60% of the world
103 river discharge and a discharge-weighted average dSi riverine concentration of 158 $\mu\text{M-Si}$
104 (Dürr et al., 2011), remains at $F_{RdSi} = 6.2 (\pm 1.8) \text{ Tmol-Si yr}^{-1}$ (Tréguer & De La Rocha, 2013).
105 However, not only dSi is transferred from the terrestrial to the riverine system, with particulate
106 Si mobilised in crystallised or amorphous forms (Dürr et al., 2011). According to Saccone et
107 al. (2007), the term "amorphous silica" (aSi) includes biogenic silica (bSi, from phytoliths,
108 freshwater diatoms, sponge spicules), altered bSi, and pedogenic silicates, the three of which
109 can have similar high solubilities and reactivities. Delivery of aSi to the fluvial system has been
110 reviewed by Frings et al. (2016) and they suggested a value of $F_{RaSi} = 1.9 (\pm 1.0) \text{ Tmol-Si yr}^{-1}$.
111 Therefore, total $F_R = 8.1 (\pm 2.0) \text{ Tmol-Si yr}^{-1}$.

Mis en forme : Non Surlignage

112 No progress has been made regarding aeolian dust deposition into the ocean (Tegen & Kohfeld,
113 2006) and subsequent release of dSi via dust dissolution in seawater since Tréguer and De La
114 Rocha (2013), which summed the flux of particulate dissolvable silica and wet deposition of

119 dSi through precipitations. Thus, our best estimate for the aeolian flux of dSi, F_A , remains 0.5
120 (± 0.5) Tmol-Si yr⁻¹.

121 2.2 Dissolution of minerals (F_w)

122 As shown in Fig. 2, the low-temperature dissolution of siliceous minerals in seawater and from
123 sediments feeds a dSi flux, F_w , through two processes: (1) the dissolution of river-derived
124 lithogenic particles deposited along the continental margins and shelves, and (2) the dissolution
125 of basaltic glass in seawater, processes that work mostly in deep waters. About 15-20 Gt yr⁻¹ of
126 river-derived lithogenic particles are deposited along the margins and shelves (e.g. Syvitskia et
127 al., 2003, also see Fig. 2). Dissolution experiments with river sediments or basaltic glass in
128 seawater showed that 0.08-0.17% of the Si in the solid phase was released within a few days to
129 months (e.g., Jones et al., 2012; Morin et al., 2015; Oelkers et al., 2011; Pearce et al., 2013).
130 However, the high solid-to-solution ratios in these experiments increased the dSi concentration
131 quickly to near-equilibrium conditions inhibiting further dissolution, which prevents direct
132 comparison with natural sediments. Field observations and subsequent modelling of Si release
133 range around 0.5 – 5% yr⁻¹ of the Si originally present in the solid phase dissolved into the
134 seawater (e.g., Arsouze et al., 2009; Jeandel and Oelkers, 2015). On the global scale, Jeandel et
135 al. (2011) estimated the total flux of dissolution of minerals to range between 0.7 - 5.4 Tmol-Si
136 yr⁻¹, i.e. similar to the dSi river flux. However, this estimate is based on the assumption of 1-
137 3% congruent dissolution of sediments for a large range of lithological composition which, so
138 far, has not been proven.

139 Another approach to estimate F_w is to consider the benthic efflux from sediments devoid of
140 biogenic silica deposits. Frings (2017) estimates that “non-biogenic silica” sediments (i.e. clays
141 and calcareous sediments, which cover about 78% of the ocean area) may contribute up to 44.9
142 Tmol-Si yr⁻¹ via a benthic diffusive Si flux. However, according to lithological descriptions
143 given in GSA Data Repository 2015271 some of the “non-biogenic silica” sediment classes
144 described in this study may contain significant bSi, which might explain this high estimate for
145 F_w . Tréguer and De La Rocha (2013) considered benthic efflux from non-siliceous sediments
146 ranging between ~10-20 mmol m⁻² yr⁻¹, in agreement with Tréguer et al. (1995). If extrapolated
147 to 120 M km² zone of opal-poor sediments in the global ocean, this gives an estimate of F_w =
148 1.9 (± 0.7) Tmol-Si yr⁻¹.

149 2.3 Submarine groundwater (F_{GW})

150 Since 2013, several papers have sought to quantify the global oceanic input of dissolved Si
151 (dSi) from submarine groundwater discharge (SGD), which includes terrestrial (freshwater) and
152 marine (saltwater) components (Fig. 2). Silicic acid inputs through SGD may be considerable,

Mis en forme : Non Surlignage

Mis en forme : Non Surlignage

Mis en forme : Non Surlignage

Supprimé:

Mis en forme : Non Surlignage

154 similar to or in excess of riverine input in some places. For instance, Georg et al. (2009)
155 estimated this input to be $0.093 \text{ Tmol-Si yr}^{-1}$ in the Bay of Bengal, which is $\sim 66\%$ of the
156 Ganges-Brahmaputra river flux of dSi to the ocean. At a global scale Tréguer and De La Rocha
157 (2013)'s best estimate for F_{GW} was $0.6 (\pm 0.6) \text{ Tmol-Si yr}^{-1}$. More recently, Rahman et al. (2019)
158 used a global terrestrial SGD flux model weighted according to aquifer lithology (Beck et al.,
159 2013) in combination with a compilation of dSi in shallow water coastal aquifers to derive a
160 terrestrial groundwater input of dSi to the world ocean of $0.7 (\pm 0.1) \text{ Tmol-Si yr}^{-1}$. This new
161 estimate, with its relatively low uncertainty, represents the lower limit flux of dSi to the ocean
162 via SGD. The marine component of SGD, driven by a range of physical processes such as
163 density gradients or waves and tides, is fed by seawater that circulates through coastal aquifers
164 or beaches via advective flow paths (Fig. 2; also see Fig. 1 of Li et al., 1999). This circulating
165 seawater may become enriched in dSi through bSi or mineral dissolution, the degree of
166 enrichment being determined by subsurface residence time and mineral type (Anschutz et al.,
167 2009; Ehlert et al. 2016a; Techer et al., 2001).

168 Several lines of evidence show that the mineral dissolution (strictly corresponding to net dSi
169 input) may be substantial (e.g., Ehlert et al., 2016b). Focusing on processes occurring in tidal
170 sands, Anschutz et al. (2009) showed that they can be a biogeochemical reactor for the Si cycle.
171 Extrapolating laboratory-based dissolution experiments performed with pure quartz, Fabre et
172 al. (2019) calculated that the potential flux of dissolution of siliceous sandy beaches **that is**
173 driven by wave and tidal action. If, according to Luijendijk et al. (2018) one-third of the world's
174 shorelines are sandy beaches, this dissolution flux could be $3.2 (\pm 1.0) \text{ Tmol Si yr}^{-1}$. However,
175 this estimate is not well constrained because it has not been validated by field experiments
176 (Supplement, section 2). Cho et al. (2018), using a ^{228}Ra inverse model and groundwater
177 $\text{dSi}/^{228}\text{Ra}$ ratios, estimate the total (terrestrial + marine) SGD dSi flux to the ocean to be $3.8 (\pm$
178 $1.0) \text{ Tmol-Si yr}^{-1}$; **this represents an upper limit value for SGD's contribution to the global**
179 ocean dSi cycle. Without systematic data that corroborates the net input of dSi through the
180 circulation of the marine component of SGD (e.g., porewater $\delta^{30}\text{Si}$, paired dSi and ^{228}Ra
181 measurements), we estimate the range of net input of dSi through total SGD as $0.7 \text{ Tmol-Si yr}^{-1}$
182 1 (Rahman et al., 2019) to $3.8 \text{ Tmol-Si yr}^{-1}$ (Cho et al., 2018), with an average, i.e. $F_{\text{GW}} = 2.3$
183 $(\pm 1.1) \text{ Tmol-Si yr}^{-1}$, which is approximately three times larger than Tréguer & De La Rocha
184 (2013).

185

186 **2.4 (Sub)polar glaciers (F_{ISMW})**

Mis en forme : Non Surlignage

Mis en forme : Non Surlignage

187 This flux was not considered by Tréguer & De La Rocha (2013). Several researchers have now
188 identified polar glaciers as sources of Si to marine environments (Tréguer, 2014; Meire et al.,
189 2016; Hawkings et al., 2017). The current best estimate of discharge weighted dSi concentration
190 in (sub)Arctic glacial meltwater rivers lies between 20-30 μM although concentrations ranging
191 between 3 and 425 μM have been reported (Graly et al., 2014; Meire et al., 2016; Hatton et al.,
192 2019). Only two values currently exist for dSi from subglacial meltwater beneath the Antarctic
193 Ice Sheet (Whillans Subglacial Lake and Mercer Subglacial Lake, 126 – 140 μM ; Michaud et
194 al., 2016, Hawkings et al., in press), and a limited dataset from periphery glaciers in the
195 McMurdo Dry Valleys and Antarctic Peninsula (~10 – 120 μM ; Hatton et al., 2020; Hirst et al.,
196 2020). Furthermore, iceberg dSi concentrations remain poorly quantified but are expected to be
197 low (~5 μM) (Meire et al., 2016). Meltwater typically contains high suspended sediment
198 concentrations, due to intense physical erosion by glaciers, with a relatively high dissolvable
199 aSi component (0.3-1.5% dry weight) equating to concentrations of 70-340 μM (Hawkings,
200 2018; Hatton et al., 2019). Iceberg aSi concentrations are lower (28-83 μM) (Hawkings et al.,
201 2017). This particulate phase appears fairly soluble in seawater (Hawkings et al., 2017) and
202 large benthic dSi fluxes in glacially influenced shelf seas have been observed (Hendry et al.,
203 2019; Ng et al., 2020). Direct silicic acid input from (sub)polar glaciers is estimated to be 0.04
204 (± 0.04) Tmol-Si yr⁻¹. If the aSi flux is considered then this may provide an additional 0.29 (\pm
205 0.22) Tmol-Si yr⁻¹, with a total F_{ISMW} (= dSi+aSi) input estimate of 0.33 (± 0.26) Tmol-Si yr⁻¹.
206 This does not include any additional flux from benthic processing of glacially derived particles
207 in the coastal regions (see section 2.2 above).

Mis en forme : Non Surlignage

Mis en forme : Non Surlignage

209 2.5 Hydrothermal activity (F_H)

210 Tréguer & De La Rocha (2013)'s estimate for F_H was 0.6 (± 0.4) Tmol-Si yr⁻¹. Seafloor
211 hydrothermal activity at mid-ocean ridges (MOR) and ridge-flanks is one of the fundamental
212 processes controlling the exchange of heat and chemical species between seawater and ocean
213 crust (Wheat & Mottl, 2000). A major challenge limiting our current models of both heat and
214 mass flux (e.g. Si flux) through the seafloor is estimating the distribution of the various forms
215 of hydrothermal fluxes, including focused (i.e. high-temperature) vs. diffuse (i.e. low
216 temperature) and ridge axis vs. ridge flank fluxes. Estimates of the Si flux for each input are
217 detailed below.

Mis en forme : Non Surlignage

218 *Axial and near axial hydrothermal fluxes settings:* The best estimate of the heat flux at ridge
219 axis (i.e. crust 0–0.1 Ma in age) is 1.8 (± 0.4) TW, while the heat flux in the near-axial region

220 (i.e. crust 0.1–1 Ma in age) has been inferred at $1.0 (\pm 0.5)$ TW (Mottl, 2003). The conversion
221 of heat flux to hydrothermal water and chemical fluxes requires assumptions regarding the
222 temperature at which this heat is removed. For an exit temperature of $350 (\pm 30)^\circ\text{C}$ typical of
223 black smoker vent fluids, and an associated enthalpy of $1,500 (\pm 190)$ J g⁻¹ at 450–1000 bars
224 and heat flux of $2.8 (\pm 0.4)$ TW, the required seawater flux is $5.9 (\pm 0.8) 10^{16}$ g yr⁻¹ (Mottl,
225 2003). High temperature hydrothermal dSi flux is calculated using a dSi concentration of $19 (\pm$
226 $11)$ mmol kg⁻¹, which is the average concentration in hydrothermal vent fluids that have an exit
227 temperature $> 300^\circ\text{C}$ (Mottl, 2012). This estimate is based on a compilation of > 100 discrete
228 vent fluid data, corrected for seawater mixing (i.e. end-member values at Mg=0, Edmond et al.,
229 1979) and phase separation. Although the chlorinity of hot springs varies widely, nearly all of
230 the reacted fluid, whether vapor or brine, must eventually exit the crust within the axial region.
231 The integrated hot spring flux must therefore have a chlorinity similar to that of seawater. The
232 relatively large range of dSi concentrations in high-temperature hydrothermal fluids likely
233 reflect the range of geological settings (e.g. fast- and slow-spreading ridges) and host-rock
234 composition (ultramafic, basaltic or felsic rocks). Because dSi enrichment in hydrothermal
235 fluids result from mineral-fluid interactions at depth, and is mainly controlled by the solubility
236 of secondary minerals such as quartz (Mottl 1983; Von Damm et al. 1991), it is also possible
237 to obtain a theoretical estimate of the concentration of dSi in global hydrothermal vent fluids.
238 Under the conditions of temperature and pressure (i.e. depth) corresponding to the base of the
239 upflow zone of high temperature ($>350 - 450^\circ\text{C}$) hydrothermal systems, dSi concentrations
240 between 16 to 22 mmol kg⁻¹ are calculated, which is in good agreement with measured values
241 in end-member hydrothermal fluids. Using a dSi concentration of $19 (\pm 3.5)$ mmol kg⁻¹ and
242 water flux of $4.8 (\pm 0.8) \times 10^{16}$ g yr⁻¹, we determine an axial hydrothermal Si flux of $0.91 (\pm$
243 $0.29)$ Tmol-Si yr⁻¹. It should be noted, however, that high-temperature hydrothermal fluids may
244 not be entirely responsible for the transport of all the axial hydrothermal heat flux (Elderfield
245 and Schultz, 1996; Nielsen et al., 2006). Because dSi concentrations in diffuse hydrothermal
246 fluids is not significantly affected by subsurface Si precipitation during cooling of the
247 hydrothermal fluid (Escoube et al., 2015), we propose that that the global hydrothermal Si flux
248 is not strongly controlled by the nature (focused vs. diffuse) of axial fluid flow.

249 *Ridge flank hydrothermal fluxes:* Chemical fluxes related to seawater-crust exchange at ridge
250 flanks has been previously determined through direct monitoring of fluids from low-
251 temperature hydrothermal circulation (Wheat and Mottl, 2000). Using basaltic formation fluids
252 from the 3.5 Ma crust on the eastern flank of the Juan de Fuca Ridge (Wheat and McManus,

Mis en forme : Non Surlignage

Code de champ modifié

Mis en forme : Non Surlignage

Mis en forme : Non Surlignage

Mis en forme : Non Surlignage

Mis en forme : Non Surlignage

Mis en forme : Non Surlignage

253 2005), a global flux of $0.011 \text{ Tmol-Si yr}^{-1}$ for warm ridge flank is calculated. This estimate is
254 based on the measured Si anomaly associated with warm spring ($0.17 \text{ mmol kg}^{-1}$) and a ridge
255 flank fluid flux determined using oceanic Mg mass balance, therefore assuming that the ocean
256 is at steady-state with respect to Mg. More recent results of basement fluid compositions in cold
257 and oxygenated ridge flank settings (e. g. North Pond, Mid-Atlantic Ridge) also confirms that
258 incipient alteration of volcanic rocks may result in significant release of Si to circulating
259 seawater (Meyer et al., 2016). The total heat flux through ridge flanks, from 1 Ma crust to a
260 sealing age of 65 Ma, has been estimated at $7.1 (\pm 2) \text{ TW}$. Considering that most of ridge-flank
261 hydrothermal power output should occur at cool sites ($< 20^\circ\text{C}$), the flux of slightly altered
262 seawater could range from 0.2 to $2 \times 10^{19} \text{ g yr}^{-1}$, rivaling with the flux of river water to the ocean
263 of $3.8 \times 10^{19} \text{ g yr}^{-1}$ (Mottl, 2003). Using this estimate and Si anomaly of $0.07 \text{ mmol-Si kg}^{-1}$
264 reported in cold ridge flank setting from North Pond (Meyer et al., 2016), a Si flux of 0.14 to
265 $1.4 \text{ Tmol-Si yr}^{-1}$ for cold ridge flank could be calculated. Because of the large volume of
266 seawater interacting with oceanic basalts in ridge flank settings, even a small chemical anomaly
267 resulting from reactions within these cold systems could result in a globally significant
268 elemental flux. Hence, additional studies are required to better determine the importance of
269 ridge flanks to oceanic Si budget.
270 Combining axial and ridge flank estimates, the best estimate for F_H is now $1.7 (\pm 0.8) \text{ Tmol-Si}$
271 yr^{-1} , approximately three times larger than the estimate from Tréguer & De La Rocha (2013).

Mis en forme : Non Surlignage

272 **2.6 Total net inputs** (Table 1A)

273 Total Si input = $8.1 (\pm 2.0) (F_{R(\text{dsi+aSi})}) + 0.5 (\pm 0.5) (F_A) + 1.9 (\pm 0.7) (F_W) + 2.3 (\pm 1.1) (F_{\text{GW}})$
274 $+ 0.3 (\pm 0.3) (F_{\text{ISMW}}) + 1.7 (\pm 0.8) (F_H) = \mathbf{14.8 (\pm 2.6) \text{ Tmol-Si yr}^{-1}}$.

275 The uncertainty of the total Si inputs (and total Si outputs, section 3) has been calculated using
276 the error propagation method from Bevington and Robinson (2003). This has been done for
277 both the total fluxes and the individual flux estimates.

Mis en forme : Non Surlignage

Mis en forme : Non Surlignage

278

279 **3. Advances in output fluxes**

280 **3.1 Long-term burial of planktonic biogenic silica in sediments (F_B)**

281 Long-term burial of bSi, which generally occurs below the top 10-20 cm of sediment, was
282 estimated by Tréguer & De La Rocha (2013) to be $6.3 (\pm 3.6) \text{ Tmol-Si yr}^{-1}$. The burial rates are
283 highest in the Southern Ocean (SO), the North Pacific Ocean, the equatorial Pacific Ocean, and
284 in the coastal and continental margin zone (CCMZ; DeMaster et al., 2002; Hou et al., 2019;
285 Rahman et al., 2017).

286 Post-depositional redistribution by processes like winnowing or focusing by bottom currents
287 can lead to under- and over-estimation of uncorrected sedimentation and burial rates. To correct
288 for these processes, the burial rates are typically normalized using the particle reactive nuclide
289 ^{230}Th method (e.g. Geibert et al., 2005). A ^{230}Th normalization of bSi burial rates has been
290 extensively used for the SO (Tréguer and De La Rocha, 2013), particularly in the “opal belt”
291 zone (Pondaven et al., 2000; DeMaster, 2002; Geibert et al., 2005). Chase et al. (2015) re-
292 estimated the SO burial flux, south of 40°S , at $2.3 (\pm 1.0) \text{ Tmol-Si yr}^{-1}$.
293 Hayes et al. (pers. comm., Hayes et al. under review) recently calculated total marine bSi burial
294 of $5.46 (\pm 1.18) \text{ Tmol-Si yr}^{-1}$, using a database that comprises 2,948 bSi concentrations of top
295 core sediments and ^{230}Th -corrected accumulation fluxes of open ocean locations $>1 \text{ km}$ in
296 depth. Hayes et al.’s ^{230}Th -corrected total burial rate is $2.68 (\pm 0.61) \text{ Tmol-Si yr}^{-1}$ south of 40°S ,
297 close to Chase et al. (2015)’s estimate for the SO. Hayes et al. do not distinguish between the
298 different analytical methods used for the determination of the bSi concentrations of these 2948
299 samples to calculate total bSi burial. These methods include alkaline digestion methods (with
300 variable protocols for correcting from lithogenic interferences e.g. DeMaster, 1981; Mortlock
301 and Froelich, 1989; Müller and Schneider, 1993), X-ray diffraction (e.g. Leinen et al., 1986),
302 X-ray fluorescence (e.g. Finney et al., 1988), Fourier-transform infra-red spectroscopy
303 (Lippold et al, 2012), and inductively coupled plasma mass spectrometry (e.g. Prakash Babu et
304 al., 2002). An international exercise calibration on the determination of bSi concentrations of
305 various sediments (Conley, 1998) concluded that the X-ray diffraction (XRD) method
306 generated bSi concentrations that were on average 24% higher than the alkaline digestion
307 methods. In order to test the influence of the XRD method on their re-estimate of total bSi
308 burial, Hayes et al. found that their re-estimate ($5.46 (\pm 1.18) \text{ Tmol-Si yr}^{-1}$), which includes
309 XRD data (~40% of the total number of data points), did not differ significantly from a re-
310 estimate that does not include XRD data points ($5.43 (\pm 1.18) \text{ Tmol-Si yr}^{-1}$). As a result, this
311 review includes Hayes et al.’s re-estimate for the open-ocean annual burial rate, i.e. $5.5 (\pm 1.2)$
312 Tmol-Si yr^{-1} .
313 The best estimate for the open-ocean total burial now becomes $2.8 (\pm 0.6) \text{ Tmol-Si yr}^{-1}$ without
314 the SO contribution ($2.7 (\pm 0.6) \text{ Tmol-Si yr}^{-1}$). This value is an excess of $1.8 \text{ Tmol-Si yr}^{-1}$ over
315 the DeMaster (2002) and Tréguer and De La Rocha (2013) estimates, which were based on 31
316 sediment cores mainly distributed in the Bering Sea, the North Pacific, the Sea of Okhotsk, and
317 the Equatorial Pacific (total area 23 M km^2), and where bSi% was determined solely using
318 alkaline digestion methods.

Supprimé: on

320 Estimates of the silica burial rates have been usually determined from carbon burial rates using
321 a Si:C ratio of 0.6 in CCMZ (DeMaster 2002). However, we now have independent estimates
322 of marine organic C and total initial bSi burial (e.g. Aller et al., 1996; Aller et al., 2008; Galy
323 et al., 2007; Rahman et al., 2016, 2017). It has been shown that the initial bSi burial in sediment
324 evolved as unaltered bSi or as authigenically formed alumino-silicate phases (Rahman et al.,
325 2017). The Si:C burial ratios of residual marine plankton post-remineralization in tropical and
326 subtropical deltaic systems are much greater (2.4 - 11) than the 0.6 Si:C burial ratio assumed
327 for continental margin deposits (DeMaster, 2002). The sedimentary Si:C preservation ratios are
328 therefore suggested to depend on differential remineralization pathways of marine bSi and C_{org}
329 under different diagenetic regimes (Aller, 2014). Partitioning of ³²Si activities between bSi and
330 mineral pools in tropical deltaic sediments indicate rapid and near-complete transformation of
331 initially deposited bSi to authigenic clay phases (Rahman et al., 2017). For example, in
332 subtropical/temperate deltaic and estuarine deposits ³²Si activities signal represent
333 approximately ~50% of initial bSi_{opal} delivery to sediments (Rahman et al., 2017). Using the
334 ³²Si technique Rahman et al. (2017) provided an updated estimate of bSi burial for the CCMZ
335 of 3.7 (± 2.1) Tmol-Si yr⁻¹, higher than the Tréguer and De La Rocha (2013) estimate of 3.3 (±
336 2.1) Tmol-Si yr⁻¹ based on the Si:C method of DeMaster (2002).

337 Combining the Hayes et al. (in review) burial rate for the open ocean zone including the SO,
338 and the Rahman et al. (2017) estimate for the CCMZ gives a revised global total burial flux,
339 F_B, of 9.2 (± 1.6) Tmol-Si yr⁻¹, 46% larger than the Tréguer and De La Rocha (2013) estimate.

340 **3.2 Deposition and long-term burial of sponge silica (F_{SP})**

341 Tréguer and De La Rocha (2013)'s estimate for F_{SP}, the net sink of sponge bSi in sediments of
342 continental margins, was 3.6 (± 3.7) Tmol Si yr⁻¹. The longevity of sponges, ranging from years
343 to millennia, temporally decouples the process of skeleton production from the process of
344 deposition to the sediments (Jochum et al., 2017). While sponges slowly accumulate bSi over
345 their long and variable lifetimes (depending on the species), the deposition to the sediments of
346 the accumulated bSi is a relatively rapid process after sponge death, lasting days to months
347 (Supplement, section 3). Tréguer and De La Rocha (2013)'s estimate was calculated as the
348 difference between the sponge dSi demand on continental shelves (3.7 (± 3.6) Tmol Si yr⁻¹) —
349 estimated from silicon consumption rates available for few sublittoral sponge species
350 (Maldonado et al., 2011) —, and the flux of dSi from the dissolution of sponge skeletons in
351 continental shelves (0.15 (± 0.15) Tmol Si yr⁻¹). This flux was tentatively estimated from the
352 rate of dSi dissolution from a rare, unique glass sponge reef at British Columbia (Canada) (Chu
353 et al., 2011) and which is unlikely to be representative of the portion of sponge bSi that dissolves

Mis en forme : Non Surlignage

Mis en forme : Non Surlignage

Mis en forme : Non Surlignage

Mis en forme : Non Surlignage

354 back as dSi after sponge death and before their burial in the sediments. To improve the estimate,
355 Maldonado et al. (2019) used microscopy to access the amount of sponge silica that was actually
356 being buried in the marine sediments using 17 sediment cores representing different marine
357 environments. The deposition of sponge bSi was found to be one order of magnitude more
358 intense in sediments of continental margins and seamounts than on continental rises and central
359 basin bottoms. The new best estimate for F_{SP} is $1.7 (\pm 1.6) \text{ Tmol-Si yr}^{-1}$, assuming that the rate
360 of sponge silica deposition in each core was approximately constant through the Holocene, i.e.
361 two times smaller than Tréguer and De La Rocha's preliminary estimate.

Supprimé: (Maldonado et al. (2019))

362 3.3 Reverse Weathering flux (F_{RW})

363 The previous estimate for this output flux, provided by Tréguer & De La Rocha (2013), $F_{RW} =$
364 $1.5 (\pm 0.5) \text{ Tmol-Si yr}^{-1}$, was determined using indirect evidence since the influence of reverse
365 weathering on the global Si cycle prior to 2013 was poorly understood. For example, reverse
366 weathering reactions at the sediment–water interface were previously thought to constitute a
367 relatively minor sink ($0.03 - 0.6 \text{ Tmol-Si yr}^{-1}$) of silica in the ocean (DeMaster, 1981). The
368 transformation of bSi to a neoformed aluminosilicate phase, or authigenic clay formation, was
369 assumed to proceed slowly ($> 10^4 - 10^5$ years) owing principally to the difficulty of
370 distinguishing the contribution of background lithogenic or detrital clays using the common
371 leachates employed to quantify bSi (DeMaster, 1981). Recent direct evidence supporting the
372 rapid formation of authigenic clays comes from tropical and subtropical deltas (Michalopoulos
373 & Aller, 1995; Rahman et al., 2016, 2017; Zhao et al., 2017) and several geochemical tools
374 show that authigenic clays may form ubiquitously in the global ocean (Baronas et al., 2017;
375 Ehlert et al., 2016a; Geilert et al., 2020; Michalopoulos & Aller, 2004; Pickering et al., 2020).
376 Activities of cosmogenic ^{32}Si ($t_{1/2} \sim 140$ yrs), incorporated into bSi in the surface ocean, provide
377 demonstrable proof of rapid reverse weathering reactions by tracking the fate of bSi upon
378 delivery to marine sediments (Rahman et al., 2016). By differentiating sedimentary bSi storage
379 between unaltered bSi ($b\text{Si}_{opal}$) and diagenetically altered bSi ($b\text{Si}_{altered}$) in the proximal coastal
380 zone, ^{32}Si activities in these pools indicate that $3.7 \text{ Tmol-Si yr}^{-1}$ is buried as unaltered $b\text{Si}_{opal}$
381 and $4.7 (\pm 2.3) \text{ Tmol-Si yr}^{-1}$ as authigenic clays ($b\text{Si}_{clay}$) on a global scale. Here, we adopt 4.7
382 Tmol-Si yr^{-1} for F_{RW} representing about three times the Tréguer & De La Rocha (2013)'s value.

Mis en forme : Non Surlignage

383 3.4 Total net output (Table 1A)

384 Total Si output = $9.2 (\pm 1.6) (F_{B(net\ deposit)}) + 4.7 (\pm 2.3) (F_{RW}) + 1.7 (\pm 1.6) (F_{SP}) = \mathbf{15.6 (\pm 2.4)}$
385 **Tmol-Si yr⁻¹.**

386

387 4. Advances in biological fluxes

389 **4.1 bSi annual pelagic production**

390 **4.1.1 from field data**

391 The last evaluation of global marine silica production was by Nelson et al. (1995) who estimated
392 global gross marine bSi pelagic production to be 240 (\pm 40) Tmol-Si yr⁻¹. Since 1995, the
393 number of field studies of bSi production (using either the ³⁰Si tracer method, Nelson & Goering
394 (1977) or the ³²Si method (Tréguer et al., 1991; Brzezinski & Phillips, 1997), has grown
395 substantially from 15 (1995) to 49 in 2019, allowing the first estimate based on empirical silica
396 production rate measurements (Fig. 3, and Supplement, section 4). It is usually assumed that
397 the silica production, as measured using the above methods, is mostly supported by diatoms,
398 with some unknown (but minor) contribution of other planktonic species.

399 The silica production rates measured during 49 field campaigns were assigned to Longhurst
400 provinces (Longhurst, 2007; Longhurst et al., 1995) based on location, with the exception of
401 the SO, where province boundaries were defined according to Tréguer & Jacques (1992).
402 Extrapolating these “time-and-space-limited” measurements of bSi spatially to a biogeographic
403 province, and annually from the bloom phenology for each province (calculated as the number
404 of days where the chlorophyll concentration is greater than the average concentration between
405 the maximum and the minimum values), results in annual silica production estimates for 26 of
406 the 56 world ocean provinces. The annual production of all provinces in a basin were averaged
407 for the “ocean basin” estimate (Table 2) and then extrapolated by basin area. The averages from
408 provinces were subdivided among coastal for the “domain” estimate (Table 2), SO, and open
409 ocean domains, and extrapolated based on the area of each domain. Averaging the “ocean
410 basin” and the “domain” annual estimates (Table 2), our best estimate for the global marine bSi
411 production is 267 (\pm 18) Tmol-Si yr⁻¹ (Table 2).

412 **4.1.2 bSi annual pelagic production from models**

413 Estimates of bSi production were also derived from satellite productivity models, and from
414 global ocean biogeochemical models (GOBMs). We used global net primary production (NPP)
415 estimates from the carbon-based productivity model (Westberry et al., 2008) and the vertically
416 generalized productivity model (VGPM) (Behrenfeld & Falkowski, 1997) for the estimates
417 based on satellite productivity models. NPP estimates from these models were divided into
418 oligotrophic (< 0.1 μ g Chl a L⁻¹), mesotrophic (0.1 - 1.0 μ g Chl a L⁻¹) and eutrophic (> 1.0 μ g
419 Chl a L⁻¹) areas (Carr et al., 2006). The fraction of productivity by diatoms in each area was
420 determined using the DARWIN model (Dutkiewicz et al., 2015) allowing a global estimate
421 where diatoms account for 29% of the production. Each category was further subdivided into
422 High Nutrient Low Chlorophyll (HNLC) zones (>5 μ M surface nitrate, Garcia et al., 2014),

Mis en forme : Non Surlignage

423 coastal zones (< 300 km from a coastline) and open ocean (remainder) zones for application of
424 Si:C ratios to convert to diatom silica production. Si:C ratios were 0.52 for HNLC regions,
425 0.065 for the open ocean and 0.13 for the coastal regions, reflecting the effect of Fe limitation
426 in HNLC areas (Franck et al., 2000), of Si limitation for uptake in the open ocean (Brzezinski
427 et al., 1998, 2011; Brzezinski & Nelson, 1996; Krause et al., 2012), and of replete conditions
428 in the coastal zone (Brzezinski, 1985). Silica production estimates were then subdivided
429 between coast (within 300 km of shore), open ocean and SO (northern boundary 43°S from
430 Australia to South America, 34.8°S from South America to Australia) and summed to produce
431 regional estimates (Table 2). Our best estimate for the global marine bSi production is 207 (\pm
432 23) Tmol-Si yr⁻¹ from satellite productivity models (Table 2).

433 A second model-based estimate of silica production used 18 numerical GOBMs models of the
434 marine silica cycle that all estimated global silica export from the surface ocean (Aumont et al.,
435 2015; Bernard et al., 2011; De Souza et al. 2014; Dunne et al., 2007; Dutkiewicz et al., 2015;
436 Gnanadesikan et al., 1999; Heinze et al., 2003; Holzer et al., 2014; Jin et al., 2006; Matsumoto
437 et al., 2013; Pasquier & Holzer, 2017; Roshan et al., 2018; Sarmiento et al., 2007; Usbeck,
438 1999; Ward et al., 2012; Wischmeyer et al., 2003). These include variants of the MOM,
439 HAMOCC OCIM, DARWIN, cGENIE and PICES models. Export production was converted
440 to gross silica production by using a silica dissolution-to-production (D:P) ratio for the surface
441 open ocean of 0.58 and 0.51 for the surface of coastal regions (Tréguer & De La Rocha, 2013).
442 Model results were first averaged within variants of the same model and then averaged across
443 models to eliminate biasing the average to any particular model. Our best estimate from
444 GOBMs for the global marine bSi production is 276 (\pm 23) Tmol-Si yr⁻¹ (Table 2). Averaging
445 the estimates calculated from satellite productivity models and GOBMs give a value of 242 (\pm
446 49) Tmol-Si yr⁻¹ for the global marine bSi production (Table 2).

447 **4.1.3 Best estimate for bSi annual pelagic production**

448 Using a simple average of the “field” and “model” estimates, the revised best estimate of global
449 marine gross bSi production, mostly due to diatoms, is now $F_{P_{gross}} = 255 (\pm 52) \text{ Tmol-Si yr}^{-1}$,
450 not significantly different from the Nelson et al. (1995)’s value.

451 In the SO, a key area for the world ocean Si cycle (DeMaster, 1981), there is some disagreement
452 among the different methods of estimating bSi production. Field studies give an estimate of 67
453 Tmol-Si yr⁻¹ for the annual gross production of silica in the SO, close to the estimate of 60
454 Tmol-Si yr⁻¹ calculated using satellite productivities models (Table 2). However, the bSi
455 production in the SO estimated by ocean biogeochemical models is about twice as high, at 129
456 Tmol-Si yr⁻¹ (Table 2). The existing in-situ bSi production estimates are too sparse to be able

Mis en forme : Non Surlignage

457 to definitively settle whether the lower estimate or the higher estimate is correct, but there is
458 reason to believe that there are potential biases in both the satellite NPP models and the ocean
459 biogeochemical models. SO chlorophyll concentrations may be underestimated by as much as
460 a factor of 3-4 (Johnson et al., 2013), which affects the NPP estimates in this region and hence
461 our bSi production estimates by this method. The bSi production estimated by ocean
462 biogeochemical models is highly sensitive to vertical exchange rates in the SO (Gnanadesikan
463 and Toggweiler, 1999), and is also dependent on the representation of phytoplankton classes in
464 models with explicit representation of phytoplankton. Models that have excessive vertical
465 exchange in the SO (Gnanadesikan and Toggweiler, 1999), or that represent all large
466 phytoplankton as diatoms, may overestimate the Si uptake by plankton in the SO. Other sources
467 of uncertainty in our bSi production estimates include poorly-constrained estimates of the Si:C
468 ratio and dissolution:production ratios (see Supplement section 4). The errors incurred by these
469 choices are more likely to cancel out in the global average, but could be significant at regional
470 scales, potentially contributing to the discrepancies in SO productivity across the various
471 methods.

472 **4.1.4 Estimates of the bSi production of other pelagic organisms**

473 Extrapolations from field and laboratory work show that the contribution of picocyanobacteria
474 (like *Synechococcus*, Baines et al. 2012, Brzezinski et al., 2017; Krause et al., 2017) to the
475 world ocean accumulation of bSi is $< 20 \text{ Tmol-Si yr}^{-1}$. The gross silica production of rhizarians,
476 siliceous protists, in the 0-1000 m layer might range between 2 – 58 Tmol-Si yr^{-1} , about 50%
477 of it occurring in the 0-200 m layer (Llopis Monferrer et al., 2020).

478 Note that these preliminary estimates of bSi accumulation or production by picocyanobacteria
479 and rhizarians are within the uncertainty of our best estimate of F_{Pgross} .

480 **4.2 Estimates of the bSi production of benthic organisms**

481 The above updated estimate of the pelagic production does not take into account bSi production
482 by benthic organisms like benthic diatoms and sponges. Our knowledge of the production terms
483 for benthic diatoms is poor and no robust estimate is available for bSi annual production of
484 benthic diatoms at global scale (Supplement, section 4).

485 Substantial progress has been made for silica deposition by siliceous sponges recently.
486 Laboratory and field studies reveal that sponges are highly inefficient in the molecular transport
487 of dSi compared to diatoms and consequently bSi production, particularly when dSi
488 concentrations are lower than $75 \mu\text{M}$, a situation that applies to most ocean areas (Maldonado
489 et al., 2020). On average, sponge communities are known to produce bSi at rates that are about
490 2 orders of magnitude smaller than those measured for diatom communities (Maldonado et al.,

Supprimé: G+T

Mis en forme : Non Surlignage

492 2012). The global standing crop of sponges is very difficult to be constrained and the annual
493 bSi production attained by such standing crop even more difficult to estimate because sponge
494 populations are not homogeneously distributed on the marine benthic environment and
495 extensive, poorly mapped and unquantified aggregations of heavily silicified sponges occur in
496 deep sea of all oceans. A first tentative estimate of bSi production for sponges on continental
497 shelves, where sponge biomass can be more easily approximated, ranged widely, from 0.87 to
498 7.39 Tmol-Si yr⁻¹, because of persisting uncertainties in estimating sponge standing crop
499 (Maldonado et al., 2012). A way to estimate the global annual bSi production by sponges
500 without knowing their standing crop is to retrace bSi production values from the amount of
501 sponge bSi that is annually being deposited to the ocean bottom, after assuming that, in the long
502 run, the standing crop of sponges in the ocean is in equilibrium (i.e, it is neither progressively
503 increasing nor decreasing over time). The deposition rate of sponge bSi has been estimated at
504 49.95 (± 74.14) mmol-Si m⁻² yr⁻¹ on continental margins, at 0.44 (± 0.37) mmol-Si m⁻² yr⁻¹ in
505 sediments of ocean basins where sponge aggregations do not occur and at 127.30 (± 105.69)
506 mmol-Si m⁻² yr⁻¹ in deep-water sponge aggregations (Maldonado et al., 2019). A corrected
507 sponge bSi deposition rate for ocean basins is estimated at 2.98 (± 1.86) mmol Si m⁻² yr⁻¹
508 assuming that sponge aggregations do not occupy more than 2% of seafloor of ocean basins
509 (Maldonado et al., 2019). A total value of 6.15 (± 5.86) Tmol-Si yr⁻¹ can be estimated for the
510 global ocean when the average sponge bSi deposition rate for continental margins and
511 seamounts (representing 108.02 Mkm² of seafloor) and for ocean basins (253.86 Mkm²) is
512 scaled up through the extension of those bottom compartments. If the bSi production being
513 accumulated as standing stock in the living sponge populations annually is assumed to become
514 constant in a long-term equilibrium state, the global annual deposition rate of sponge bSi can
515 be considered as a reliable estimate of the minimum value that the annual bSi production by the
516 sponges can reach in the global ocean. The large associated SD value does not derive from the
517 approach being unreliable but from the spatial distribution of the sponges on the marine bottom
518 being extremely heterogeneous, with some ocean areas being very rich in sponges and sponge
519 bSi in sediments at different spatial scales while other areas are completely deprived from these
520 organisms.

521

522 5. Discussion

523 5.1 Overall residence times

524 The overall geological residence time for Si in the ocean (τ_G) is equal to the total amount of dSi
525 in the ocean divided by the net input (or output) flux. We re-estimate the total ocean dSi

Mis en forme : Non Surlignage

Mis en forme : Non Surlignage

526 inventory value derived from the Pandora model (Peng et al. 1993), which according to Tréguer
527 et al. (1995) was 97,000 Tmol-Si. An updated estimate of the global marine dSi inventory was
528 computed by interpolating the objectively analyzed annual mean silicate concentrations from
529 the 2018 World Ocean Atlas (Garcia et al., 2019) to the OCIM model grid (Roshan et al., 2018).
530 Our estimate is now 120,000 Tmol-Si, i.e. about 24 % higher than the Tréguer et al. (1995)
531 estimate. Tables 1B and 3 show updated estimates of τ_G from Tréguer et al. (1995) and Tréguer
532 & De La Rocha (2013) using this updated estimate of the total dSi inventory into account. Our
533 updated budget (Fig. 1, Table 1B, Table 3A) reduces past estimates of τ_G (Tréguer et al., 1995;
534 Tréguer and De La Rocha, 2013) by more than half, from ca.18 kyr to ca. 8 kyr (Table 3C).
535 This brings the ocean residence time of Si closer to that of nitrogen (< 3 kyr, Sarmiento &
536 Gruber, 2006) than phosphorus (30 – 50 kyr, Sarmiento & Gruber, 2006).

537 The overall biological residence time, τ_B , is calculated by dividing the total dSi content of the
538 world ocean by gross silica production. It is calculated from the bSi pelagic production only
539 given the large uncertainty on our estimate of the bSi production by sponges. τ_B is ca. 470 years
540 (Table 1B, Table 3). Thus, Si delivered to the ocean passes through the biological uptake and
541 dissolution cycle on average 16 times (τ_G / τ_B) before being removed to the sea floor (Table 1B,
542 Table 3C).

543 The new estimate for the global average preservation efficiency of bSi buried in sediments is
544 $(F_B = 9.2 / F_{P_{gross}} = 255) = 3.6 \%$, similar to the Tréguer and De La Rocha (2013) estimate,
545 making bSi in sediments an intriguing potential proxy for export production (Tréguer et al.,
546 2018). Note that the reverse weathering flux (F_{RW}) is also fed by the export flux (F_E), (Fig. 4).
547 So, the preservation ratio of biogenic silica in sediment can be calculated as $F_B + F_{RW} / F_{P_{gross}}$
548 $= 13.9 / 255 = 5.45\%$, which is ~30 times larger than the carbon preservation efficiency.

549 **5.2 The issue of steady state**

550 Over a given time scale, an elemental cycle is at steady state if the outputs balance the inputs
551 in the ocean and the mean concentration of the dissolved element remains constant.

552 **5.2.1 Long time scales ($>\tau_G$)**

553 Over geologic time scales, the average dSi concentration of the ocean has undergone drastic
554 changes. A seminal work (Siever, 1991) on the biological – geochemical interplay of the Si
555 cycle showed a factor of 100 decline in ocean dSi concentration from 550 Myr to the present.
556 This decline was marked by the rise of silicifiers like radiolarian and sponges during the
557 Phanerozoic. Then during the mid-Cenozoic diatoms started to dominate a Si cycle previously
558 controlled by inorganic and diagenetic processes. Conley et al., (2017) hypothesized that
559 biological processes might also have influenced the dSi concentration of the ocean at the start

Mis en forme : Non Surlignage

Supprimé :

561 of oxygenic photosynthesis taking into account the impact of the evolution of biosilicifying
 562 organisms (including bacterial-related metabolism). There are further evidence that the existing
 563 lineages of sponges have their origin in ancient (Mesozoic) oceans with much higher dSi
 564 concentrations than the modern ocean. Some recent sponge species can only complete their
 565 silica skeletons if dSi concentration much higher than those in their natural habitat are provided
 566 experimentally (Maldonado et al., 1999). Also, all recent sponge species investigated to date
 567 have kinetics of dSi consumption that reach their maximum speed only at dSi concentrations
 568 that are one to two orders of magnitude higher than the current dSi availability in the sponge
 569 habitats, indicating that the sponge physiology evolved in dSi-richer, ancestral scenarios. Note
 570 that with a geological residence time of Si of ca. 8,000 years, the Si cycle can fluctuate over
 571 glacial-interglacial time scale.

572 5.2.2 Short time scales (< τ_G)

573 In the modern ocean the main control over silica burial and authigenic formation rate is the bSi
 574 production rate of pelagic and benthic silicifiers, as shown above. The gross production of bSi
 575 due to diatoms depends on the dSi availability in the surface layer (Fig. 1). Silicic acid does not
 576 appear to be limiting in several zones of the world ocean, which include the coastal zones, and
 577 the HNLC zones (Tréguer & De La Rocha, 2013). Note that any short-term change of dSi inputs
 578 does not imply modification of bSi production, nor export, nor burial rate. For this reason,
 579 climatic changes or anthropogenic impacts that affect dSi inputs to the ocean by rivers and/or
 580 other pathways, could lead to an imbalance of Si inputs and outputs in the modern ocean.

581 5.2.3 A possible steady-state scenario

582 Within the limits of uncertainty, the total net inputs of dSi and aSi are $14.8 (\pm 2.6)$ Tmol-Si yr⁻¹
 583 and are approximately balanced by the total net output flux of Si of $15.6 (\pm 2.4)$ Tmol-Si yr⁻¹.
 584 Fig. 1 supports the hypothesis that the modern ocean Si cycle is at steady state, compatible with
 585 the geochemical and biological fluxes of Table 1.

586 Consistent with Fig. 1, Fig. 4 shows a steady-state scenario for the Si cycle in the coastal and
 587 continental margins zone (CCMZ), often called the “boundary exchange” zone which,
 588 according to Jeandel (2016) and Jeandel & Oelkers (2015), plays a major role in the land-to-
 589 ocean transfer of material (also see Fig. 2). Fig. 4 illustrates the interconnection between
 590 geochemical and biological Si fluxes, particularly in the CCMZ. In agreement with Laruelle et
 591 al. (2009), Fig. 4 also shows that the “open ocean” bSi production is mostly fueled by dSi inputs
 592 from below (92.5 Tmol-Si yr⁻¹) and not by the CCMZ (4.7 Tmol-Si yr⁻¹) (Supplemental section
 593 5).

594 5.3 The impacts of global change on the Si cycle

Supprimé:).

Mis en forme : Non Surlignage

Supprimé: (

Supprimé: +

Mis en forme : Non Surlignage

Supprimé:)

Supprimé: Si

Mis en forme : Non Surlignage

Supprimé: Thus, on short timescales, there are no strong negative feedbacks between supply rates and production or burial rates, which would necessarily keep the marine Si cycle in balance

Mis en forme : Non Surlignage

Supprimé: For this reason

Mis en forme : Non Surlignage

Supprimé: shows a possible scenario for the Si cycle at steady state in the modern ocean, based on a balance of inputs and outputs at 15.6 Tmol-Si yr⁻¹,

Supprimé: Raising the mean input flux up to 15.6 Tmol-Si yr⁻¹ makes sense because of potential underestimation of different components of the present best-estimate total input. For instance, as shown in section 2 our present estimate of F_{gw} (submarine groundwater) is not well constrained as we do not know the contribution of the marine component and of the dSi flux engendered by the dissolution of siliceous sands in the tidal zone (section 2.3). ¶

Supprimé: possible

Mis en forme : Non Surlignage

Supprimé: 5.3 Specific cases and unresolved questions ¶ In the past three decades our best estimates for the net inputs or outputs of Si in and from the world ocean (Tréguer et al., 1995; Tréguer & De La Rocha, 2013) have increased by a factor of two. This is not only due to better spatial and temporal coverage of Si stocks and fluxes in the different regions of the world ocean, but also due to a better understanding of the processes that control the Si cycle, such as SGD, reverse weathering, and particulate Si inputs (see discussion above). The two case studies herein presented illustrate the need to further improve our understanding of the different contributions of dSi inputs in the coastal zone and the deep Pacific Ocean. ¶

5.3.1 Chinese seas¶

In many respects the Chinese marginal seas, composed of the Bohai Sea (BS), Yellow Sea (YS), East China Sea (ECS), and South China Sea (SCS), are a unique and interesting system to study the cycling of Si in the marine environment. First, the dSi SGD inputs largely exceed the dSi riverine inputs by a factor of about 3-16 times for the BS, YS, and ECS (e.g. Ding et al., 2019; Liu et al., 2017a; Liu et al., 2017b; Wang et al. (...)

Mis en forme : Non Surlignage

Mis en forme : Non Surlignage

Mis en forme : Non Surlignage

Mis en forme : Non Surlignage

Supprimé: 4

717 As illustrated by Fig. 1 and 4, the pelagic bSi production is mostly fueled from the large, deep
718 ocean recycled pool of dSi. This lengthens the response time of the Si cycle to changes in dSi
719 inputs to the ocean due to global change (including climatic and anthropogenic effects),
720 increasing the possibility for the Si cycle to be out of balance.

721 **5.3.1 Impacts on riverine inputs of dSi and aSi**

722 Climate change at short time scale during the 21st century impacts the ocean delivery of riverine
723 inputs of dSi and aSi (F_R) and of the terrestrial component of the submarine groundwater
724 discharge (F_{GW}), either directly (e.g. dSi and aSi weathering and transport), or indirectly by
725 affecting forestry and agricultural dSi export. So far the impacts of climate change on the
726 terrestrial Si cycle have been reported for boreal wetlands (Struyf et al., 2010), North American
727 (Opalinka & Cowling, 2015) and western Canadian Arctic rivers (Phillips, 2020), and the
728 tributaries of the Laptev and East Siberian Seas (Charette et al., 2020), but not for tropical
729 environments. Tropical watersheds are the key areas for the transfer of terrestrial dSi to the
730 ocean, as approximately 74% of the riverine Si input is from these regions (Tréguer et al., 1995).

731 Precipitation in tropical regions usually follow “the rich-get-richer” mechanism in a warming
732 climate according to model predictions (Chou et al., 2004, 2008). In other words, in tropical
733 convergence zones rainfall increases with climatological precipitation, but the opposite is true
734 in tropical subsidence regions, creating diverging impacts for the weathering of tropical soils.
735 If predictions of global temperature increase and variations in precipitations of the IPCC are
736 correct (IPCC, 2018) it is uncertain how F_R or F_{GW} , two major components of dSi and aSi
737 inputs, will change. Consistent with these considerations are the conclusions of Phillips (2020)
738 on the impacts of climate change on the riverine delivery of dSi to the ocean, using machine-
739 learning based approach. Phillips (2020) predicts that within the end of this century dSi mean
740 yield could increase regionally (for instance in the Arctic region), but the global mean dSi yield
741 is projected to decrease, using a model based on 30 environmental variables including
742 temperature, precipitation, land cover, lithology, and terrain.

743 **5.3.2 Abundance of marine and pelagic and benthic silicifiers**

744 A change in diatom abundance was not seen on the North Atlantic from Continuous Plankton
745 Recorder (CPR) data over the period 1960-2009 (Hinder et al., 2012). However, studies have
746 cautioned that many fields (e.g. Chl) will take several decades before these changes can be
747 measured precisely beyond natural variability (Henson et al 2010; Dutkiewicz et al 2019). The
748 melting of Antarctic ice platforms has already been noticed to trigger impressive population
749 blooms of highly silicified sponges (Fillinger et al. 2013).

750 **5.3.3. Predictions for the ocean phytoplankton production and bSi production**

Supprimé: 4

Mis en forme : Non Surlignage

Mis en forme : Non Surlignage

Mis en forme : Non Surlignage

Supprimé: 4

Mis en forme : Non Surlignage

Supprimé: 4

754 Twenty-first century climate change will affect ocean circulation, stratification and upwelling,
755 and therefore nutrient cycling (Aumont et al., 2003; Bopp et al., 2005, 2013). With increased
756 stratification dSi supply from upwelling will reduce (Fig. 1 and 4) leading to less siliceous
757 phytoplankton production in surface compartments of lower latitudes and possibly the North
758 Atlantic (Tréguer et al., 2018). The impact of climate change on the phytoplankton production
759 in polar seas is highly debated as melting of sea ice decreases light limitation. In the Arctic
760 Ocean an increase in nutrient supply from river- and shelf derived waters (at the least for silicic
761 acid) will occur through the Transpolar Drift potentially impacting rates of primary production,
762 including bSi production (e.g. Charette et al., 2020). In the SO bSi production may increase in
763 the coastal and continental shelf zone as iron availability increases due to ice sheet melt and
764 iceberg delivery (Duprat et al., 2016; Herraiz-Borreguero et al., 2016; Boyd et al., 2016;
765 Hutchins & Boyd, 2016; Tréguer et al., 2018; Hawkings et al., in press). However, Henley et al
766 (2019) suggests a shift from diatoms to haptophytes and cryptophytes with changes in ice
767 coverage in the Western Antarctic Peninsula. How such changes in coastal environments and
768 nutrient supplies will interplay is unknown. Globally, it is very likely that a warmer and more
769 acidic ocean alters the pelagic bSi production rates, thus modifying the export production and
770 outputs of Si at short time scales.

771 Although uncertainty is substantial, modelling studies (Bopp et al., 2005; Dutkiewicz et al.,
772 2019; Laufkötter et al, 2015) suggest regional shifts in bSi pelagic production with climatic
773 change. These models predict a global decrease in diatom biomass and productivity over the
774 the 21st century (Bopp et al., 2005, Dutkiewicz et al., 2019, Laufkötter et al., 2015), which
775 would lead to a reduction in the pelagic biological flux of silica. Regional responses differ, with
776 most models suggesting a decrease in diatom productivity in the lower latitudes and many
777 predicting an increase in diatom productivity in the SO (Laufkötter et al, 2015). Holzer et al.
778 (2019) suggest that changes in supply of dFe will alter bSi production mainly by inducing
779 floristic shifts, not by relieving kinetic limitation. Increased primary productivity is predicted
780 to come from a reduction in sea-ice area, faster growth rates in warmer waters and longer
781 growing seasons in the high latitudes. However, many models have very simple ecosystems
782 including only diatoms and a small phytoplankton. In these models, increased primary
783 production in the SO is mostly from diatoms. Models with more complex ecosystem
784 representations (i.e. including additional phytoplankton groups) suggest that increased primary
785 productivity in the future SO will be due to other phytoplankton types (e.g. pico-eukaryote) and
786 that diatoms biomass will decrease (Dutkiewicz et al, 2019; also see model PlankTOM5.3 in
787 Laufkötter et al, 2015), except in regions where sea-ice cover has reduced. Differences in the

Mis en forme : Non Surlignage

788 complexity of the ecosystem and parameterizations, in particular in terms of temperature
789 dependences of biological process, between models lead to widely varying predictions
790 (Dutkiewicz et al., 2019; Laufkotter et al., 2015). These uncertainties suggest we should be
791 cautious in our predictions of what will happen with the silica biogeochemical cycle in a future
792 ocean.

793 **5.5 Other anthropogenic impacts**

794 For decades if not centuries, anthropogenic activities directly or indirectly altered the Si cycle
795 in rivers, and the CCMZ (Bernard et al., 2010; Conley et al. 1993; Derry et al. 2005; Humborg
796 et al., 2006; Ittekkot et al., 2000, 2006; Laruelle et al. 2009; Liu et al., 2012; Yang et al., 2015;
797 Wang et al., 2018; Zhang et al., 2019). Processes involved include eutrophication and pollution
798 (Conley et al., 1993; Liu et al., 2012), river damming (Ittekkot, 2006; Ittekkot et al., 2000; Yang
799 et al., 2015; Wang et al., 2018), deforestation (Conley, 2008), changes in weathering and in
800 river discharge (Bernard et al. 2010; Yang et al. 2015), and deposition load in river deltas (Yang
801 et al., 2015).

802 Among these processes, river damming is known for having the most spectacular and short
803 time-scale impacts on the Si delivery to the ocean. River damming favours enhanced
804 biologically mediated absorption of dSi in the dam reservoir, thus resulting in significant
805 decreases in dSi concentration downstream. Drastic perturbations on the Si-cycle and
806 downstream ecosystem have been shown (Ittekkot, 2006; Ittekkot et al. 2000; Humborg et al.
807 2006; Zhang, 2019), particularly downstream of the Nile (Mediterranean Sea), the Danube
808 (Black Sea) and the fluvial system of the Baltic Sea. Damming is a critical issue for major rivers
809 of the tropical zone (Amazon, Congo, Changjiang, Huanghe, Ganges, Brahmaputra, etc.),
810 which carry 74 % of the global exorheic dSi flux (Dürr et al., 2011; Tréguer et al., 1995). Among
811 these major rivers, the course of Amazon and Congo are, so far, not affected by a dam or, if so
812 for the Congo river, the consequence of Congo damming for the Si cycle in the equatorial african
813 coastal system has not been studied. The case for Changjiang (Yangtze), one of the major world
814 players on dSi delivery to the ocean, is of particular interest. Interestingly, the Changjiang
815 (Yangtze) river dSi concentrations decreased dramatically from 1960s to 2000 (before the
816 building of the Three Gorges Dam, TGD). This decrease is attributed to a combination of
817 natural and anthropogenic impacts (Wang et al., 2018a). Paradoxically, since the construction
818 of the TGD (2006 - 2009) no evidence of additional retention of dSi by the dam has been
819 demonstrated (Wang et al., 2018a).

820 « Over the 21st century, the influence of climate change, and other anthropogenic
821 modifications, will have variable impacts on the regional and global biogeochemical cycling of

Mis en forme : Non Surlignage

822 Si. The input of dSi will likely increase in specific regions (e.g. Arctic Ocean), whilst inputs to
823 the global ocean might decrease. Global warming will increase stratification of the surface
824 ocean, leading to a decrease of dSi inputs from the deep sea, although this is unlikely to
825 influence the Southern Ocean (see Section 5.3.3). Model-based predictions suggest a global
826 decrease in diatom production, with a subsequent decrease in export production and Si burial
827 rate. Clearly, new observations are needed to validate model predictions.

Supprimé: ¶

829 6. Conclusions/recommendations

830 The main question that still needs to be addressed is whether the contemporary marine Si
831 cycle is at steady state, which requires the uncertainty in total inputs and outputs to be
832 minimized.

Mis en forme : Non Surlignage

833 For the input fluxes, more effort is required to quantify groundwater input fluxes, particularly
834 using geochemical techniques to identify the recycled marine flux from other processes that
835 generate a net input of dSi to the ocean. In light of laboratory experiments by Fabre et al. (2019)
836 demonstrating low temperature dissolution of quartz in clastic sand beaches, collective
837 multinational effort should examine whether sandy beaches are major global dSi sources to the
838 ocean. Studies addressing uncertainties at the regional scale are critically needed. Further, better
839 constraints on hydrothermal inputs (for the North-East Pacific specific case), aeolian input and
840 subsequent dissolution of minerals both in the coastal and in open ocean zones, and inputs from
841 ice melt in polar regions are required.

Supprimé: address to

842 For the output fluxes, it is clear that the alkaline digestion of biogenic silica (DeMaster, 1981;
843 Mortlock & Froelich, 1989, Müller and Schneider, 1993), one of the commonly used methods
844 for bSi determination in sediments, is not always effective at digesting all the bSi present in
845 sediments. This is especially true for highly silicified diatom frustules, radiolarian tests, or
846 sponge spicules (Maldonado et al., 2019; Pickering et al. 2020). Quantitative determination of
847 bSi is particularly difficult for lithogenic or silicate-rich sediments (e.g. estuarine and coastal
848 zones), for example those of the Chinese seas. An analytical effort for the quantitative
849 determination of bSi from a variety of sediment sources and the organization of an international
850 comparative analytical exercise are of high priority for future research. It is also clear that
851 reverse weathering processes are important not only in estuarine or coastal environments, but
852 also in distal coastal zones, slope, and open ocean regions of the global ocean (Baronas et al.,
853 2017; Ehlert et al., 2016a; Geilert et al., 2020; Michalopoulos & Aller, 2014; Pickering et al.,
854 2020; Chong et al., 2016). Careful use of geochemical tools (e.g. ^{32}Si , Ge/Si, $\delta^{30}\text{Si}$; Pickering et
855 al., 2020; Geilert et al., 2020; Ehlert et al., 2016; Ng et al., 2019; Cassarino et al., in press) to

Mis en forme : Non Surlignage

Mis en forme : Non Surlignage

858 trace partitioning of bSi between opal and authigenic clay phases may further elucidate the
859 magnitude of this sink, particularly in understudied areas of the ocean.

860 This review highlights the significant progress that has been made in the past decade toward
861 improving our quantitative and qualitative understanding of the sources, sinks and internal
862 fluxes of the marine Si cycle. Filling the knowledge gaps identified in this review is also
863 essential if we are to anticipate changes in the Si cycle, and their ecological and biogeochemical
864 impacts, in the future ocean.

865
866 *Data availability:* All data used in this review article are available in the referenced articles.
867 Data of biogenic pelagic production are shown in Supplement (Annex 1).

868
869 *Supplement:* The supplement related to this article is available on line at...XXX

870
871 *Author contributions.* PJT & JNS defined the manuscript content and wrote the paper. MAC,
872 CE, JH, SR, OR & PT wrote the inputs section. JS, CE, SR, & MM wrote the outputs section.
873 MB, TD, SD, AL, & PT wrote the pelagic production section. MLA & MM wrote the sponge
874 subsections. SML, LR, & PT wrote the discussion section. Every author re-read and approved
875 the review article.

876
877 *Competing interests.* The authors declare that they have no conflict of interest.

878
879 *Acknowledgements.* The idea for this manuscript was conceived during a conference of the
880 SILICAMICS Network, held in June 2018 at the University of Victoria (Canada). This work
881 was supported by the French National Research Agency (18-CEO1-0011-01), and by the
882 Spanish Ministry of Science, Innovation and Universities (PID2019-108627RB-I00). Thanks
883 are due to Sébastien Hervé (LEMAR-IUEM, Plouzané) for his art work.

884
885 **References**
886 Aller, R. C., Blair, N.E., Xia, Q., & Rude, P.D.: Remineralization rates, recycling, and storage
887 of carbon in Amazon shelf sediments, *Cont. Shelf Res.*, 16, 753–786, 1996.
888 Aller, R.C.: Sedimentary diagenesis, depositional environments, and benthic fluxes, in: *Treatise*
889 *on Geochemistry: Second edition*, edited by: Holland, H.D., & Turekian, K.K.,

890 Elsevier, Oxford, 8, 293–334, 2014.

891 Aller, R.C., Blair, N.E., & Brunskill, G.J.: Early diagenetic cycling, incineration, and burial of
892 sedimentary organic carbon in the central Gulf of Papua (Papua New Guinea), *J.*
893 *Geophys. Res. Earth Surf.*, 113, 1-22, 2008.

894 Anschutz, P., Smith, T., Mouret, A., Deborde, J., Bujan, S., Poirier, D., Lecroart, P.: Tidal sands
895 as biogeochemical reactors, *Estuar. Coast. Shelf Sci.*, 84, 84–90, 2009.

896 Bevington, P.R., Robinson, D.K., 2003. *Data Reduction and Error Analysis for the Physical*
897 *Sciences*, third ed., McGrawHill, NewYork, 2003.

898 Arsouze, T., Dutay, J. C., Lacan, F., & Jeandel, C.: Reconstructing the Nd oceanic cycle using
899 a coupled dynamical - biogeochemical model. *Biogeosciences*, 6, 2829-2846, 2009.

900 Aumont, O., Ethé, C., Tagliabue, A., Bopp, L., & Gehlen, M.: PISCES-v2, an ocean
901 biogeochemical model for carbon and ecosystem studies, *Geosci. Model Dev.*, 8, 2465–
902 2513, 2015.

903 Aumont, O., Maier-Reimer, E., Blain, S., & Monfray, P.: An ecosystem model of the global
904 ocean including Fe, Si, P co-limitations, *Glob. Biogeochem. Cycles*, 17, 1060,
905 doi:10.1029/2001GB001745, 2003.

906 Baines, S.B., Twining, B.S., Brzezinski, M.A., Krause, J.W., Vogt, S., Assael, D., McDaniel,
907 H.: Significant silicon accumulation by marine picocyanobacteria, *Nat. Geosci.*, 5, 886–
908 891, 2012.

909 Baronas, J.J., Hammond, D.E., McManus, J., Wheat, C.G., & Siebert, C.A.: Global Ge isotope
910 budget, *Geochim. Cosmochim. Acta*, 203, 265-83, 2017.

911 Beck, A. J., Charette, M. A., Cochran, J. K., Gonneea, M. E., Peucker-Ehrenbrink, B.:
912 Dissolved strontium in the subterranean estuary - Implications for the marine strontium
913 isotope budget. *Geochim. Cosmochim. Acta*. 117, 33–52, 2013.

914 Behrenfeld, M. J., & Falkowski, P. G.: Photosynthetic rates derived from satellite-based
915 chlorophyll concentration, *Limnol. Oceanogr.*, 42, 1-20, 1997.

916 Bernard, C.Y., Dürr, H.H., Heinze, C., Segsneider, J., & Maier-Reimer, E.: Contribution of
917 riverine nutrients to the silicon biogeochemistry of the global ocean – a model study,
918 *Biogeosciences*, 8, 551–564, 2011.

919 Bernard, C.Y., Laruelle, G.G., Slomp, C.P., & Heinze, C.: Impact of changes in river fluxes on
920 silica on the global marine silicon cycle: a model comparison, *Biogeosciences*, 7, 4441-
921 453, 2010.

922 Berner, R.A., Lasaga, A.C., Garrels, R.M.: The carbonate-silicate geochemical cycle and its
923 effect on atmospheric carbon dioxide over the past 100 millions years. *Am. J. Sci.*, 283,

924 641–683, 1983.

925 Bopp, L., Resplandy, L., Orr, J.C., Doney, S.C., Dunne, J.P., Gehlen, M., Halloran, P., Heinze,
926 C., Ilyina, S  f  rian, R., Tjiputra, J., M. Vichi, M.: Multiple stressors of ocean
927 ecosystems in the 21st century: Projections with CMIP5 models, *Biogeosciences*, 10,
928 6225-6245, 2013.

929 Bopp, L., Aumont, O., Cadule, P., Alvain, S., Gehlen, G.: Response of diatoms distribution to
930 global warming and potential implications: A global model study, *Geophys. Res. Lett.*,
931 32, L19606, 2005.

932 Boyd, P.W., Cornwall, C.E., Davison, A., Doney, S.C., Fourquez, M., Hurd, C.L., Lima, I.D.,
933 McMin, A.: Biological responses to environmental heterogeneity under future ocean
934 conditions, *Glob. Change Biol.*, 22, 2633-2650, 2016.

935 Brzezinski, M.A., Krause, J.W., Baines, S.B., Collier, J.L., Ohnemus, D.C., Twining, B.S. :
936 Patterns and regulation of silicon accumulation in *Synechococcus* spp., *J. Phycol.* 53,
937 746–761, 2017.

938 Brzezinski, M.A., Baines, S.B., Balch, W.M., Beucher, C.P., Chai, F., Dugdale, R.C., Krause,
939 J.W., Landry, M.R., Marchi, A., Measures, C.I., Nelson, D.M., Parker, A.E., Poulton,
940 A.J., Selph, K.E., Strutton, P.G., Taylor, A.G., Twining, B.S.: Twining, Co-limitation
941 of diatoms by iron and silicic acid in the equatorial Pacific, *Deep Sea Res. Part II Top.*
942 *Stud. Oceanogr.*, 58, 493–511, 2011.

943 Brzezinski, M.A.: The Si:C:N ratio of marine diatoms: Interspecific variability and the effect
944 of some environmental variables, *J. Phycol.*, 21, 347–357, 1985.

945 Brzezinski, M.A. & Nelson, D.M.: Chronic substrate limitation of silicic acid uptake rates in
946 the western Sargasso Sea. *Deep Sea Res. Part II Top. Stud. Oceanogr.*, 43, 437–453,
947 1996.

948 Brzezinski, M.A., & Phillips, D.R.: Evaluation of ³²Si as a tracer for measuring silica
949 production rates in marine waters, *Limnol. Oceanogr.*, 42, 856–865, 1997.

950 Brzezinski, M.A., Villareal, T.A., & Lipschultz, F.: Silica production and the contribution of
951 diatoms to new and primary production in the central North Pacific, *Mar. Ecol. Prog.*
952 *Ser.*, 167, 89–104, 1998.

953 Carr, M., Friedrichs, A.M., Schmeltz, M., Aita, M.N, Antoine, A., Arrigo, K.R., Asanuma, I,
954 Aumont, O, Barber, R., Behrenfeld, M., Bidigare, R., Buitenhuis, E.T., Campbell, J.,
955 Ciotti, A., Dierssen, H., Dowell, M., Dunne, J., Esaias, W, et al.: A comparison of global
956 estimates of marine primary production from ocean color, *Deep Sea Res. Part II Top.*
957 *Stud. Oceanogr.*, 53, 741–770 (2006).

958 [Cassarino, L., Hendry, K. R., Henley, S. F., MacDonald, E., Arndt, S., Sales de Freitas, F., Pike,](#)
959 [J., Firing, Y.L. : Sedimentary nutrient supply in productive hotspots off the West](#)
960 [Antarctic Peninsula revealed by silicon isotopes. *Glob. Biogeochem. Cycles*, in press.](#)

961 Charette M.A., Kipp, L.E., Jensen, L.T., Dabrowski, J.S., Whitmore, L.M., Fitzsimmons, J.N.,
962 Williford, T., Ulfsbo, A., Jones, E., Bundy, R. : The Transpolar Drift as a Source of
963 Riverine and Shelf-Derived Trace Elements to the Central Arctic Ocean, *J. G. R.*
964 *Oceans*, 125, [e2019JC015920], 2020, DOI:10.1029/2019jc015920

965 Chase, Z., Kohfeld, K.E., Matsumoto, K.: Controls on biogenic silica burial in the Southern
966 Ocean, *Glob. Biogeochem. Cycles*, 29, 1599–1616, 2015.

967 Cho, H.-M., Kim, G., Kwon, E.Y., Moosdorf, N., Garcia-Orellana, J., Santos, I.R.: Radium
968 tracing nutrient inputs through submarine groundwater discharge in the global ocean,
969 *Sci. Rep.*, 8, 2439, 2018.

970 Chong, L.S., Berelson, W., Hammond, D.E., Fleisher, M.Q., Anderson, R.F., Rollins, N.E.,
971 Lund, S.: Biogenic sedimentation and geochemical properties of deep-sea sediments of
972 the Demerara slope/abyssal Plain: Influence of the Amazon River Plume, *Mar. Geol.*,
973 379, 124-139, 2016.

974 Chou, C. & Neelin, J.D.: Mechanisms of global warming impacts on regional tropical
975 precipitations, *J. Clim.*, 17, 2688-2701, 2004.

976 Chou, C., Neelin, J.D., Chen, C.-A., & Tu, J.-Y.: Evaluating the “rich-get-richer” mechanism
977 in tropical precipitation change under global warming, *J. Clim.*, 22, 1982-2005, 2008.

978 Conley, D.J.: An interlaboratory comparison for the measurement of biogenic silica in
979 sediments, *Mar. Chem.*, 63, 39-48, 1988.

980 Conley, D.J., Likens, G.E., Buso, D.C., Saccone, L., Bailey, S.W., Johnson, C.E.: Deforestation
981 causes increased dissolved silicate losses in the Hubbard Brook Experimental Forest,
982 *Glob. Change Biol.*, 14, 2458-2554, 2008.

983 Conley, D.J., Frings, P.J., Fontorbe, G., Clymans, W., Stadmark, J., Hendry, K.R., Marron,
984 A.O., De La Rocha, C.L.: Biosilicification drives a decline of dissolved Si in the oceans
985 through geologic time, *Front. Mar. Sci.*, 4, 397, 2017.

986 Conley, D.J., Schelske, C.L., & Stoermer, E.F.: Modification of the biogeochemical of silica
987 with eutrophication, *Mar. Ecol. Progr. Ser.*, 101, 179-192, 1993.

988 De Souza, G.F., Slater, R.D., Dunne, J.P., & Sarmiento, J.L.: Deconvolving the controls on the
989 deep ocean’s silicon stable isotope distribution, *Earth Planet. Sci. Lett.*, 398, 66–76,
990 2014.

991 DeMaster, D.J.: The accumulation and cycling of biogenic silica in the Southern Ocean:

992 revisiting the marine silica budget, *Deep Sea Res. Part II Top. Stud. Oceanogr.*, 49,
993 3155–3167, 2002.

994 DeMaster, D.J.: The supply and accumulation of silica in the marine environment, *Geochim.*
995 *Cosmochim. Acta*, 45, 1715-1732, 1981.

996 Derry, L.A., Kurtz, A.C., Ziegler, K., & Chadwick, O.A.: Biological control of terrestrial silica
997 cycling and export fluxes to watershed, *Nature*, 433, 728-731, 2005.

998 Ding, S., Chen, P., Liu, S.M., Zhang, G., Zhang, J., Dan, S.F.: Nutrient dynamics in the
999 Changjiang and retention effect in the Three Gorges Reservoir. *J. Hydrol.*, 574, 96–109,
1000 2019.

1001 Dunne, J.P., Sarmiento, J.L., & Gnanadesikan, A.: A synthesis of global particle export from
1002 the surface ocean and cycling through the ocean interior and on the seafloor, *Glob.*
1003 *Biogeochem. Cycles*, 21, GB4006 , 2007.

1004 Duprat, L.P.A.M., Bigg, G.R., Winton, D.J.: Enhanced Southern Ocean marine productivity
1005 due to fertilization by giant icebergs, *Nature Geosci.*, 9, 219-221, 2016.

1006 Dürr H.H., Meybeck, M., Hartmann, J, Laruelle, G.G., & Roubeix, V.: Global spatial
1007 distribution of natural riverine silica inputs to the coastal zone, *Biogeosciences*, 8, 597–
1008 620, 2011.

1009 Dutkiewicz, S., Hickman, E., Jahn, O., Henson, S., Beaulieu, B. & Monier, E.: Ocean colour
1010 signature of climate change, *Nat. Comm.*, 10, 019, 2019.

1011 Dutkiewicz, S., Hickman, A.E., Jahn, O., Gregg, W.W., Mouw, C.B., & Follows, M.J.:
1012 Capturing optically important constituents and properties in a marine biogeochemical
1013 and ecosystem model, *Biogeosciences*, 12, 4447–4481, 2015.

1014 Edmond, J.M., Measures, C., Mangum, B., Grant, B., F. R. Sclater, F. R., Collier, R., Hudson,
1015 A., Gordon, L. I., Corliss, J. B.: On the formation of metal-rich deposits at ridge crests,
1016 *Earth. Planet. Sci. Lett.*, 46, 19-30, 1979.

1017 Ehlert, C., Doeringa, K. Wallmanna, K., Scholza, F., Sommera, S., Grasse, P., Geilert, S.,
1018 Frank, M.: Stable silicon isotope signatures of marine pore waters – Biogenic opal
1019 dissolution versus authigenic clay mineral formation, *Geochim. Cosmochim. Acta*, 191,
1020 102–117, 2016a.

1021 Ehlert, C., Reckhardt, A., Greskowiak, J., Liguori, B.T.P., Böning, P., Paffratha, R., Brumsack,
1022 H.-J., Pahnke, K.: Transformation of silicon in a sandy beach ecosystem: insights from
1023 stable silicon isotopes from fresh and saline groundwaters, *Chem. Geol.*, 440, 207–218,
1024 2016b.

1025 Elderfield, H. & Schultz, A.: Mid-ocean ridge hydrothermal fluxes and the chemical

1026 composition of the ocean, *Ann. Rev. Earth Planet. Sci.*, 24, 191-224, 1996.

1027 Escoube, R., Rouxel, O., Edwards, K., Glazer, B. and Donard, O.: Coupled Ge/Si and Ge
1028 isotope ratios as geochemical tracers of seafloor hydrothermal systems: case studies at
1029 Loihi Seamount and East Pacific Rise 9°50'N. *Geochim. Cosmochim. Acta*, 167, 93-
1030 112, 2015.

1031 Fabre, S., Jeandel, C., Zambardi, T., Roustan, M., & Almar, R.: An overlooked silica source of
1032 the modern oceans: are sandy beaches the key? *Front. Earth Sci.*, 7, 231, 2019.

1033 Fillinger, L., Janussen, D., Lundälv, T., Richter, C.: Rapid glass sponge expansion after climate-
1034 induced Antarctic ice shelf collapse, *Curr. Biol.*, 23, 1330-1334, 2013.

1035 Finney, B.P., Lyle, M.W., Heath, G.R.: Sedimentation at MANOP Site H (eastern equatorial
1036 Pacific) over the past 400,000 years: Climatically induced redox variations and their
1037 effects on transition metal cycling, *Paleoceanogr.*, 1988.
1038 <https://doi.org/10.1029/PA003i002p00169>

1039 Franck, V.M., Brzezinski, M.A., Coale, K.H., & Nelson, D.M.: Iron and silicic acid
1040 concentrations regulate Si uptake north and south of the Polar Frontal Zone in the Pacific
1041 Sector of the Southern Ocean, *Deep. Res. Part II Top. Stud. Oceanogr.*, 47, 3315–3338,
1042 2000.

1043 Frings, P.: Revisiting the dissolution of biogenic Si in marine sediments: a key term in the ocean
1044 Si budget, *Acta Geochim.*, 36, 429–432, 2017.

1045 Frings, P.J., Clymans, W., Fontorbe, G., De La Rocha, C.L., & Conley, D.J.: The continental
1046 Si cycle and its impact on the ocean Si isotope budget. *Chem. Geol.*, 425, 12–36, 2016.

1047 Galy, V.C., France-Lanord, C., Beysac, O., Faure, P., Kudrass, H., & Pahol, F.: Efficient
1048 organic carbon burial in the Bengal fan sustained by the Himalayan erosional system,
1049 *Nature*, 450, 407-410, 2007.

1050 Garcia, H. E., Locarnini, R.A., Boyer, T.P., Antonov, J.I., Baranova, O.K., Zweng, M.M.,
1051 Reagan, J.R., & Johnson, D.R.: Dissolved Inorganic Nutrients (phosphate, nitrate,
1052 silicate), in: *World Ocean Atlas 2013*, edited by Levitus, Mishonov A., NOAA Atlas
1053 NESDIS 76, 25 pp., 2014.

1054 Garcia, H.E., Weathers, K.W., Paver, C.R., Smolyar, I., Boyer, T.P., Locarnini, M.M., Zweng,
1055 M.M., Mishonov, A.V., Baranova, O.K., Seidov, D., Reagan, J.R.: Dissolved Inorganic
1056 Nutrients (phosphate, nitrate, silicate), in: *World Ocean Atlas 2018*, edited by Levitus,
1057 Mishonov A., NOAA Atlas NESDIS 84, 35 pp., 2019,
1058 https://data.nodc.noaa.gov/woa/WOA18/DOC/woa18_vol4.pdf

1059 Geibert, W., Rutgers van der Loeff, M.M., Usbeck, R., Gersonde, R., Kuhn, G., Seeberg-
1060 Elverfeldt, J.: Quantifying the opal belt in the Atlantic and southeast Pacific sector of
1061 the Southern Ocean by means of ^{230}Th normalization, *Glob. Biogeochem. Cycles*, 19,
1062 GB4001, 2005.

1063 Geilert, S., Grasse, P., Wallmann, K., Liebetrau, V., Menzies, C.D.: Serpentine alteration as
1064 source of high dissolved silicon and elevated $\delta^{30}\text{Si}$ values to the marine Si cycle, *Nature*
1065 *comm.*, 2020. <https://doi.org/10.1038/s41467-020-18804-y>

1066 Georg, R.B., West, A.J., Basu, A.R., & Halliday, A.N.: Silicon fluxes and isotope composition
1067 of direct groundwater discharge into the Bay of Bengal and the effect on the global
1068 ocean silicon isotope budget, *Earth Plant. Sci. Lett.*, 203, 67-74, 2009.

1069 Gnanadesikan, A., & Toggweiler, J.R.: Constraints placed by silicon cycling on vertical
1070 exchange in general circulation models. *Geophys. Res. Lett.*, 26, 1865–1868, 1999.

1071 Graly, J.A., Humphrey, N.F., Landowski, C.M., Tarper, J.T.: Chemical weathering under the
1072 Greenland Ice Sheet, *Geology*, 42, 551-554, 2014.

1073 Hatton, J.E., Hendry, K.R., Hawkings, J.R., Wadham, J.L., Kohler, T.J., Stibal, M., Beaton,
1074 A.D., Bagshaw, E.A., Telling, J.: Investigation of subglacial weathering under the
1075 Greenland Ice Sheet using silicon isotopes, *Geochim. Cosmochim. Acta*, 247, 191–206,
1076 2019.

1077 Hatton, J.E., Hendry, K.R., Hirst, C., Opfergelt, S., Henkel, S., Silva-Busso, A., Welch, S.A.,
1078 Wadham, J.L., Lyons, W.B., Bagsaw, E., Staubwasser, M., McKnight, D.: Silicon
1079 Isotopic Composition of Dry and Wet-Based Glaciers in Antarctica, *Frontiers Earth Sci.*,
1080 8 (286), 2020. doi: 10.3389/feart.2020.00286

1081 Hautala, S., Hammond, D.E.: Abyssal pathways and the double maximum in the northeast
1082 Pacific basin. *Geophys. Res. Lett.*, 2020. 10.1029/2020GL089010

1083 Hawkings, J. R., Hatton, J.E., Hendry, K. R., de Souza, G. F., Wadham, J. L., Ivanovic, R.,
1084 Kohler, T. J., Stibal, M., Beaton, A., Lamarche-Gagnon, G., Tedstone, A., Hain, M. P.,
1085 Bagshaw, E., Pike, J., Tranter, M.: The silicon cycle impacted by past ice sheets, *Nat.*
1086 *Commun.*, 9, 3210, 2018.

1087 Hawkings, J.R., Wadham, J.L., Benning, L.G., Hendry, K.R., Tranter, M., Tedstone, A.,
1088 Nienow, P. & Raiswell, R. : Ice sheets as a missing source of silica to the polar oceans.
1089 *Nat. Commun.*, 8, 14198, 2017.

1090 Hawkings, J. R., Skidmore, M. L., Wadham, J. L., Priscu, J. C., Morton, P. L., Hatton, J. E.,
1091 Gardner, C. B., Kohler, T. J., Stibal, M., Bagshaw, E. A., Steigmeyer, A., Barker, J.,
1092 Dore, J. E., Lyons, W. B., Tranter, M., Spencer, R. G. M. (2020) Enhanced trace element

Mis en forme : Non Surlignage

1093 mobilization by the Earth's ice sheets, *Proceedings of the National Academy of Science*,
1094 2020. DOI: 10.1073/pnas.2014378117.

1095 Hayes, C.T., Costa, K.M., Anderson, R.F., Calvo, E., Chase Z., Demina L.L., Dutay, J.-C.,
1096 German, C.R., Heimbürger-Boavida, L.-E., Jaccard, S.L., Jacob, A., Kohfeld, K.E.,
1097 Kravchishina, M.D., Lippold, J., Mekik, F., Missiaen, L., Pavia, F.J., Paytan, A.,
1098 Pamies, Pedrosa-Pamies, R., Petrova, M.V., Rahman, S., Robinson L.F., Roy-Barman,
1099 M., Sanchez-Vidal, A., Shiller, A., Tagliabue, A., Tessin, A.C., van Hulten, M., Zhang
1100 J.: Global ocean sediment composition and burial flux in the deep sea, *Glob. Biogeo.*
1101 *Cy.* (under review).

1102 Heinze, C., Hupe, A., Maier-Reimer, E., Dittert, N., and Ragueneau, O.: Sensitivity of the
1103 marine biospheric Si cycle for biogeochemical parameter variations, *Global*
1104 *Biogeochem. Cy.*, 17, 1086, doi:10.1029/2002GB001943, 2003.

1105 Hendry, K.R., Huvenne, V.A.I., Robinson, L.F., Annett, A., Badger, M., Jacobel, A.W, Ng,
1106 H.C., Opher, J., Pickering, R.A., Taylor, M.L., Bates, S.L., Cooper, Z., Cusham, G.G.,
1107 Goodwin, C., Hoy, S., Rowland, G., Samperiz, A., Williams, J.A., Woodward, M.S. :
1108 The biogeochemical impact of glacial meltwater from Southwest Greenland, *Progress*
1109 *in Oceanogr.*, 2019. doi: <https://doi.org/10.1016/j.pocean.2019.102126>

1110 Henley, S.F., Schofield, O.M., Hendry, K.R., Schloss, I.R., Steinberg, D.K, Moffath, C., Peck,
1111 L.S., Costa, D.P., Bakker, D.C.E., Hughes, C., Rozema, P.D., Ducklow, H.W., Abele,
1112 D., Stefels, J., Van Leeuwe, M.A., Brussaard, C.P.D., Buma, A.G.J., Kohu, J., Sahade,
1113 R., Friedlaender, A.S., Stammerjohn, S.E., Venables, H.J., Meredith, M.P.: Variability
1114 and change in the west Antarctic Peninsula marine system: Research priorities and
1115 opportunities, *Progr. Oceanogr.*, 173, 208_237, 2019.

1116 Henson, S. A., Sarmiento, J. L., Dunne, J. P., Bopp, L., Lima, I., Doney, S. C., John, J.,
1117 Beaulieu, C.: Detection of anthropogenic climate change in satellite records of ocean
1118 chlorophyll and productivity, *Biogeosciences*, 7, 621–640, 2010.

1119 Herraiz-Borreguero, L., Lannuzel, D., van der Merwe, P., Treverrow, A., Pedro, J.B.: Large
1120 flux of iron from the Amery Ice Shelf marine ice to Prydz Bay, East Antarctica, *J.*
1121 *Geophys. Res.: Oceans*, 121, 6009-6020, 2016.

1122 Hinder, S. L., Hays, G. C., Edwards, M., Roberts, E. C., Walne, A. W., Gravenor, M. B.:
1123 Changes in marine dinoflagellate and diatom abundance under climate change, *Nat.*
1124 *Clim. Chang.*, 2, 271–275, 2012.

1125 Hirst, C., Opfergelt, S., Gaspard, F., Hendry, K.R., Hatton, J.E., Welch, S., McKnight, D.M.,
1126 Lyons, W.B. : Silicon Isotopes Reveal a Non-glacial Source of Silicon to Crescent

1127 Stream, McMurdo Dry Valleys, Antarctica, *Frontiers Earth Sci.*, 8 (229), 2020. doi:
 1128 10.3389/feart.2020.00229

1129 Holzer, M., Primeau, F.W., DeVries, T., & Matear, R.: The Southern Ocean silicon trap: Data-
 1130 constrained estimates of regenerated silicic acid, trapping efficiencies, and global
 1131 transport paths, *J. Geophys. Res. Ocean*, 119, 313–33, 2014.

1132 Hou Y., Hammond, D. E.; Berelson, W.M.; Kemnitz, N.; Adkins, J.F.; Lunstrum, A.: Spatial
 1133 patterns of benthic silica flux in the North Pacific reflect upper ocean production, *Deep-
 1134 Sea Research Part I*, 148, 25–33, 2019.

1135 Humborg C., Pastuszak, M., Aigars, J., H. Siegmund, H., Mörth, C.-M., Ittekkot, V.: Decreased
 1136 silica land-sea fluxes through damming in the Baltic Sea catchment –significance of
 1137 particle trapping and hydrological alteration, *Biogeochemistry* 77, 265-281, 2006.

1138 Hutchins, D.A. & Boyd, P.W.: Marine phytoplankton and the changing ocean iron cycle. *Nat.*
 1139 *Clim. Change*, 6, 1072-1076, 2016.

1140 IPCC 2018 [https://www.ipcc.ch/2018/10/08/summary-for-policymakers-of-ipcc-special-
 1141 report-on-global-warming-of-1-5c-approved-by-governments/](https://www.ipcc.ch/2018/10/08/summary-for-policymakers-of-ipcc-special-report-on-global-warming-of-1-5c-approved-by-governments/)

1142 Ittekkot, V, Humborg C, Schäfer P.: Hydrological alternations and marine biogeochemistry: a
 1143 silicate issue? *BioScience*, 50, 776–82, 2000.

1144 Ittekkot, V., Unger, D., Humborg, C., Tac An, N. T. (Eds): *The Silicon Cycle: Human
 1145 Perturbations and Impacts on Aquatic Systems*, *Comm. Probl. Environ. (SCOPE) Ser.*
 1146 *Vol. 66*. Washington, DC: Island. 296 pp, 2006.

1147 Jeandel, C.: Overview of the mechanisms that could explain the ‘Boundary Exchange’ at the
 1148 land–ocean contact, *Philos. Trans. R. Soc. A Math. Phys. Eng. Sci.*, 374, 20150287,
 1149 2016.

1150 Jeandel, C., Peucker-Ehrenbrink B., Jones, M.T., Pearce, C.R., Oelkers, E.H., Godderis, Y.,
 1151 Lacan, F., Aumont, O., Arsouze, T. : Ocean margins : the missing term for oceanic
 1152 element budgets ? *Eos Trans. AGU*, 92, 217, 2011.

1153 Jeandel, C. & Oelkers, E.H.: The influence of terrigenous particulate material dissolution on
 1154 ocean chemistry and global elements cycles, *Chem. Geol.*, 395, 50-56, 2015.

1155 Jin, X., Gruber, N. Dunne, J.P., Sarmiento, J.L., & Armstrong R.A.: Diagnosing the
 1156 contribution of phytoplankton functional groups to the production and export of
 1157 particulate organic carbon, CaCO₃, and opal from global nutrient and alkalinity
 1158 distributions, *Glob. Biogeochem. Cycles*, 20, GB2015, 2006.

1159 Jochum, K. P., Schuessler, J.A., Wang, X.-H., Stoll, B., Weis, U., Müller, W.E.G., Haug, G.H.,

1160 Andreae, M.O., Froelich, P.N.: Whole-ocean changes in silica and Ge/Si ratios during
 1161 the last deglacial deduced from long-lived giant glass sponges, *Geophys. Res. Lett.*, 44,
 1162 555-564, 2017.

1163 Johnson, R., Strutton, P.G., Wright, S.W., McMinn, A., Meiner, K.M.: Three improved satellite
 1164 chlorophyll algorithms for the Southern Ocean, *J. Geophys. Res. Oceans*, 118, 3694–
 1165 3703, 2013. doi:10.1002/jgrc.20270

1166 Johnson, H.P., Hautala, S.L., Bjorklund, T.A., Zarnetske, M.R.: Quantifying the North Pacific
 1167 silica plume, *Geoch. Geophys. Geosyst.*, 2006. <https://doi.org/10.1029/2005GC001065>

1168 Jones, M., Pearce, C.R., Oelkers, E.H.: An experimental study of the interaction of basaltic
 1169 riverine particulate material and seawater *Geochim. Cosmochim. Acta*, 77, 108-120,
 1170 2012.

1171 Krause, J.W., Mark A. Brzezinski, M.A., Baines, S.B., Collier, J.L., Twining, B.S., Ohnemus,
 1172 D.C.: Picoplankton contribution to biogenic silica stocks and production rates in the
 1173 Sargasso Sea, *Glob. Biogeochem. Cycles*, 31, 762–774, 2017.

1174 Krause, J.W., Brzezinski, M.A., Villareal, T.A., & Wilson, W.: Increased kinetic efficiency for
 1175 silicic acid uptake as a driver of summer diatom blooms in the North Pacific subtropical
 1176 gyre, *Limnol. Oceanogr.*, 57, 1084–1098, 2012.

1177 Laruelle, G.G., Roubex, V., Sferratore, A., Brodherr, B., Ciuffa, D., Conley, D.J., Dürr, H.H.,
 1178 Garnier, J., Lancelot, Le Thi Phuong, Q., Meunier, J.-D., Meybeck, M.,
 1179 Michalopoulos, P., Moriceau, B., Ní Longphuirt, S., Loucaides, S., Papush, L., Presti,
 1180 M., Ragueneau, O., Regnier, P.A.G., Saccone, L., Slomp, C.P., , Spiteri, C., Van
 1181 Cappelle, P. : Anthropogenic perturbations of the silicon cycle at the global scale: key
 1182 role of the land-ocean transition, *Glob. Biogeochem. Cycles*, 23, GB4031, 1-17, 2009.

1183 Laufkötter, C., Vogt, M., Gruber, Aita-Noguchi, M., Aumont, O., Bopp, L., Buitenhuis, E.,
 1184 Doney, S.C., Dunne, J., Hashioka, T., Hauck, J., Hirata, T., John, J., Le Quéré, C., Lima,
 1185 I.D., NakanoH., Seferian, R., Totterdell, I., Vichi, M., Völker, C.: Divers and
 1186 uncertainties of future global marine primary production in marine ecosystem models,
 1187 *Biogeosciences*, 12, 6955–6984, 2015.

1188 Leinen, M., Cwienk, D., Heath, G.R., Biscaye, P.E., Kolla, V., Thiede, J., Dauphin, J.P.:
 1189 Distribution of biogenic silica and quartz in recent deep-sea sediments, *Geology*, 14,
 1190 199–203, 1986

1191 Li, D., Dong, M., Liu, S., Chen, H., & Yao, Q.: Distribution and budget of biogenic silica in
 1192 the Yangtze Estuary and its adjacent sea, *Sci. Total Environ*, 669, 590–599 (2019).

1193 Li, L, Barry, D.A., Stagnitti, F., & Parlange, J.Y.: Submarine groundwater discharge and

Mis en forme : Non Surlignage

Code de champ modifié

Mis en forme : Non Surlignage

Mis en forme : Non Surlignage

1194 associated chemical input to a coastal sea, *Water Resources Res.*, 35, 3253-3259, 1999.

1195 Lippold, J., Luo, Y., Francois, R., Allen, S.E., Gherardi, J., Pichat, S., Hickey, B., Schulz, H.:
 1196 Strength and geometry of the glacial Atlantic Meridional Overturning Circulation,
 1197 *Nature Geosci.*, 5, 813–816, 2012.

1198 Liu, J., Du, J., & Yi, L.: Ra tracer-based study of submarine groundwater discharge and
 1199 associated nutrient fluxes into the Bohai Sea, China: A highly human-affected marginal
 1200 sea, *J. Geophys. Res. Ocean*, 122, 8646–8660, 2017a.

1201 Liu, J., Su, N., Wang, X., & Du, J.: Submarine groundwater discharge and associated nutrient
 1202 fluxes into the Southern Yellow Sea: A case study for semi-enclosed and oligotrophic
 1203 seas-implication for green tide bloom, *J. Geophys. Res. Ocean*, 122, 139–152, 2017b.

1204 Liu, J., Zang, J., Bouwman, L., Liu, S., Yu, Z., Ran, X.: Distribution and budget of dissolved
 1205 and biogenic silica in the Bohai Sea and Yellow Sea, *Biogeochemistry*, 130, 85–101
 1206 2016.

1207 Liu, S.M., L.W., Zhang, G.L., Liu, Z., Yu, Z., & Ren, J.L.: Impacts of human activities on
 1208 nutrient transports in the Huanghe (Yellow River) Estuary, *J. Hydrol.*, 430-431, 103-
 1209 110, 2012.

1210 Liu, S.M., Zhang, J., & Li, R.X.: Ecological significance of biogenic silica in the East China
 1211 Sea, *Mar. Ecol. Prog. Ser.*, 290, 15–26, 2005.

1212 Llopis Monferrer, N., Boltovskoy, D., Tréguer, P., Méndez Sandin, M., Not, F., Leynaert, A.:
 1213 Estimating biogenic silica production of Rhizaria in the global ocean, *Glob.*
 1214 *Biogeochem. Cycles*, 34, e2019GB006286, 2020.

1215 Longhurst, A., S. Sathyendranath, T. Platt, Caverhill, C.: An estimate of global primary
 1216 production in the ocean from satellite radiometer data, *J. Plankton Res.*, 17, 1245–1271,
 1217 1995.

1218 Longhurst, A.R. (Ed.) : *Ecological Geography of the Sea*, Academic Press, London, ed. 2nd,
 1219 2007.

1220 Luijendijk, A., Hagenaars, G., Roshanka, R., Baart, F., Donchyts, G., Aarninkhof, S.: The state
 1221 of the world’s beaches, *Sci. Rep.*, 8, 6641, 2018.

1222 Maldonado M., Navarro L., Grasa A., Gonzalez A., Vaquerizo I.: Silicon uptake by sponges: a
 1223 twist to understanding nutrient cycling on continental margins, *Sci. Rep.*, 1, 30, 2011.

1224 Maldonado, M., Ribes, M. & van Duyl, F. C.: Nutrient fluxes through sponges, *Adv. Mar.*
 1225 *Biol.*, 62, 113–182, 2012.

1226 Maldonado, M., López-Acosta, M., Beazley, L., Kenchington, E., Koutsouveli, V., Riesgo, A.:
 1227 Cooperation between passive and active silicon transporters clarifies the ecophysiology

1228 and evolution of biosilicification in sponges. *Sci. Advances*, 6, 2020.

1229 Maldonado, M., López-Acosta, M., Sitjà, C., García-Puig, M., Galobart, C., Ercilla, G.,
1230 Leynaert, A.: Sponge skeletons as an important sink of silicon in the global oceans, *Nat.*
1231 *Geosci.* 12, 815–822, 2019.

1232 Matsumoto, K., Tokos, K., Huston, A., & Joy-Warren, H.: MESMO 2: a mechanistic marine
1233 silica cycle and coupling to a simple terrestrial scheme, *Geosci. Model Dev.* 6, 477–
1234 494, 2013.

1235 Meire, L., Meire, P., Struyf, E., Krawczyk, D.W., Arendt, K.E., Yde, J.C., Pedersen, T.J.,
1236 Hopwood, M.J., Rysgaard, S., Meysman, F.J.R.: High export of dissolved silica from the
1237 Greenland Ice Sheet, *Geophys. Res. Lett.* 43, 9173–9182, 2016.

1238 Meyer, J. L., Jaekel, U., Tully, B. J., Glazer, B. T., Wheat, C. G., Lin, H.-T., Hsieh, C.-C.,
1239 Cowen, J. P., Hulme, S. M., Girguis, P. R., Huber, J. A.: A distinct and active bacterial
1240 community in cold oxygenated fluids circulating beneath the western flank of the Mid-
1241 Atlantic ridge, *Sci. Rep.*, 6, 22541, 2016.

1242 Michalopoulos, P., & Aller, R. C.: Rapid Clay Mineral Formation in Amazon Delta Sediments:
1243 Reverse Weathering and Oceanic Elemental Cycles. *Science*, 270, 614–617, 1995.

1244 Michalopoulos, P. & Aller, R.C.: Early diagenesis of biogenic silica in the Amazon delta:
1245 alteration, authigenic clay formation, and storage, *Geochim. Cosmochim. Acta*, 68,
1246 1061–1085, 2004.

1247 Michaud, A. B., Skidmore, M. L., Mitchell, A. C., Vick-Majors, T. J., Barbante, C., Turetta,
1248 C., VanGelder, W., Priscu, J. C.: Solute sources and geochemical processes in
1249 Subglacial Lake Whillans, West Antarctica, *Geology*, 44, 347–350, 2016.

1250 Moriceau, B., Gehlen, M., Tréguer, P., Baines, S., Livage, J., André, L.: Editorial:
1251 Biogeochemistry and genomics of silicification and silicifiers, *Front. Mar. Sci.* 6, 57,
1252 2019.

1253 Morin, G.P., Vigier, N., & Verney-Carron, A.: Enhanced dissolution of basaltic glass in
1254 brackish waters: Impact on biogeochemical cycles, *Earth Planet. Sci. Lett.*, 417, 1–8,
1255 2015.

1256 Mortlock, R.A., Froelich, P.N.: A simple method for the rapid determination of biogenic opal
1257 in pelagic marine sediments, *Deep Sea Res. Part A. Oceanogr. Res. Papers*, 36, 1415–
1258 1426, 1989.

1259 Mottl, M.J.: Hydrothermal processes at seafloor spreading centers: application of basalt-
1260 seawater experimental results. In: Rona, P.A., Boström, K., Laubier, L., Smith, K.L.
1261 (eds) *Hydrothermal Processes at Seafloor Spreading Centers*. NATO Conference Series

1262 (IV Marine Sciences), 12. Springer, Boston, MA. , 1983. <https://doi.org/10.1007/978-1->
1263 4899-0402-7_10

1264 Mottl, M.J.: Partitioning of energy and mass fluxes between mid-ocean ridge axes and flanks
1265 at high and low temperature, in: Energy and Mass Transfer in Marine Hydrothermal
1266 Systems, edited by Halbach, P.E., Tunnicliffe, V., Hein, J.R., Dahlem University Press,
1267 pp. 271–286, 2003.

1268 Mottl, M. : Explanatory notes and master chemical item spreadsheet for the VentDB Data
1269 collections housed in the EarthChem Library, Version 1.0. Interdisciplinary Earth Data
1270 Alliance (IEDA), 2012. <https://doi.org/10.1594/IEDA/100207>.

1271 Müller, J., Schneider, R.: An automated leaching method for the determination of opal in
1272 sediments and particulate matter, Deep Sea Res. Part I, 40, 425-444, 1993.

1273 Nelson, D.M., & Goering, J.J.: Near-surface silica dissolution in the upwelling region off
1274 northwest Africa, Deep Sea Res., 24, 65–73, 1977.

1275 Nelson, D.M., Tréguer, P., Brzezinski, M.A., Leynaert, A., & Quéguiner, B.: Production and
1276 dissolution of biogenic silica in the ocean - Revised global estimates, comparison with
1277 regional data and relationship to biogenic sedimentation, Glob. Biogeochem. Cycles, 9,
1278 359–372, 1995.

1279 Ng, H.C., Cassarino, L., Pickering, R.A., Woodward, E.M.S., Hendry, K.R.: Sediment efflux
1280 of silicon on the Greenland margin and implications for the marine silicon cycle. Earth
1281 Planet Sci. Lett., 529, 115877, 2020.

1282 Nielsen, S. G., Rehkämper, M., Teagle, D. A. H., Butterfield, D. A., Alt, J. C. Halliday, A. N.:
1283 Hydrothermal fluid fluxes calculated from the isotopic mass balance of thallium in the
1284 ocean crust, Earth Planet. Sci. Lett., 251, 120–133, 2006.

1285 Oelkers, E. H., Gislason, S. R., Eiríksdóttir, E. S., Jones, M. T., Pearce, C. R., Jeandel C.: The
1286 role of riverine particulate material on the global cycles of the elements, Appl.
1287 Geochem., 26, S365–S369, 2011.

1288 Ohnemus, D.C., Rauschenberg, S., Krause, J.W., Brezinski, M.A.: Silicon content of individual
1289 cells of *Synechococcus* from the North Atlantic Ocean, Mar. Chem., 187, 16–24, 2016.

1290 Opalinka, B. & Cowlings, S.A.: Modelling the movement of biogenic silica from terrestrial
1291 vegetation to riverine systems within the continental USA, Ecol. Model., 312, 104-113,
1292 2015. <https://doi.org/10.1016/j.ecolmodel.2015.05.012>

1293 Pasquier, B., & Holzer, M.: Inverse-model estimates of the ocean’s coupled phosphorus,
1294 silicon, and iron cycles, Biogeosciences, 14, 4125–4159, 2017.

1295 Pearce, C.R., Jones, M.T., b, Oelkers, E.H., Pradoux, C., Jeandel, C.: The effect of particulate

1296 dissolution on the neodymium (Nd) isotope and Rare Earth Element (REE) composition
1297 of seawater, *Earth Planet. Sci. Lett.*, 369-370, 138-147, 2013.

1298 Peng, T.-S. , Maier-Reimer, E., Broecker, W.S.: Distribution of ^{32}Si in the world ocean: model
1299 compared to observation. *Glob. Biogeochem. Cycles*, 7, 464-474, 1993.

1300 Philipps, A. Modelling riverine dissolved silica on different spatial and temporal scales using
1301 statistical and machine learning methods, Ph.D thesis, Univ. Toronto, 121 pp., 2020.
1302 <http://hdl.handle.net/1807/101210>

1303 Pickering, R.A., Cassarino, L., Hendry, K.R., Wang, X.L., Maiti, K., Krause, J.W.: Using Stable
1304 Isotopes to Disentangle Marine Sedimentary Signals in Reactive Silicon Pools,
1305 *Geophys. Res. Lett.*, 2020. <https://doi.org/10.1029/2020GL087877>

1306 Pondaven, P., Ragueneau, O., Tréguer, P., Hauvespre, A., Dezileau, L., Reyss, J.L.: Resolving
1307 the 'opal paradox' in the Southern Ocean, *Nature*, 405, 168-172, 2000.

1308 Prakash Babu, C., Brumsack, J., Böttcher, M.E.: Barium as a productivity proxy in continental
1309 margin sediments: a study from the eastern Arabian Sea, *Mar. Geol.*, 184, 189-206,
1310 2002.

1311 Rahman, S., Aller, R.C., Cochran, & J.K.: Cosmogenic ^{32}Si as a tracer of biogenic silica burial
1312 and diagenesis: Major deltaic sinks in the silica cycle, *Geophys. Res. Lett.*, 43, 7124–
1313 7132, 2016.

1314 Rahman, S., Aller, R.C., & Cochran, J.K.: The missing silica sink: revisiting the marine
1315 sedimentary Si cycle using cosmogenic ^{32}Si , *Glob. Biogeochem. Cycles*, 31, 1559–
1316 1578, 2017.

1317 Rahman, S., Tamborski, J.J., Charette, M.A., & Cochran, J.K.: Dissolved silica in the
1318 subterranean estuary and the impact of submarine groundwater discharge on the global
1319 marine silica budget, *Mar. Chem.*, 208, 29–42, 2019.

1320 Roshan, S., DeVries, T., Wu, J., & Chen, G.: The internal cycling of Zinc in the ocean, *Glob.*
1321 *Biogeochem. Cycles*, 32, 1833–1849, 2018.

1322 Saconne, L., Conley, D.J., Koning, E., Sauer, D., Sommer, M., Kaczorek, D., Blecher, S.W.,
1323 Kelly, E.F.: Assessing the extraction and quantification of amorphous silica in soils of
1324 forests and grassland ecosystems. *Eur. J. Soil Sci.*, 58, 1446-1459, 2007.

1325 Sarmiento, J.L. & Gruber, N. : *Ocean biogeochemical dynamics*, Princeton University press,
1326 Princeton & Oxford, 2006.

1327 Sarmiento, J.L., Simeon, J., Gnanadesikan, A., Gruber, N., Key, R.M., Schlitzer, R.: Deep
1328 ocean biogeochemistry of silicic acid and nitrate. *Glob. Biogeochem. Cycles*, 21,
1329 GB1S90, 2007.

1330 Siever, R.: Silica in the oceans: biological – geochemical interplay, in “Scientists in Gaia”,
1331 edited by : Schneider, S.H. Boston, P.J., MIT Press, 285-295, 1991.

1332 Struyf, E., Mörth, C.-M., Humborg, C., Conley, D.J.: An enormous amorphous silica stock in
1333 boreal wetlands, *J.G.R.*, 115, G04008, 2010. doi:10.1029/2010JG001324.

1334 Syvitskia, J.P.M., Peckhama, S.D., Hilbermana, R., Mulderb, T.: Predicting the terrestrial flux
1335 of sediment to the global ocean:a planetary perspective, *Sedim. Geol.*, 162, 5–24, 2003.

1336 Talley, L.D., Joyce, T.M.: The double silica maximum in the North Pacific. *J. Geophys. Res.*,
1337 97, 5465-5480, 1992.

1338 Techer, I., Advocat, T., Lancelot, J., & Liotard, J.M.: Dissolution kinetics of basaltic glasses:
1339 Control by solution chemistry and protective effect of the alteration film, *Chem. Geol.*,
1340 176, 235–263, 2001.

1341 Tegen, I. & Kohfeld, K.E.: Atmospheric Transport of Silicon, in: The silica cycle, human
1342 perturbations and impacts on aquatic systems, edited by Ittekkot V. et al. anthropic, *Scope*
1343 66, 2006.

1344 Tréguer P. & Jacques, G.: Dynamics of nutrients and phytoplankton, and fluxes of carbon,
1345 nitrogen and silica in the Antarctic ocean, *Pol. Biol.*, 12, 149-162, 1992.

1346 Tréguer, P., Louis Lindner, L., van Bennekom, A.J., Leynaert, A., Panouse, M., Jacques, G.:
1347 Production of biogenic silica in the Weddell-Scotia Seas measured with ³²Si, *Limnol.*
1348 *Oceanogr.*, 36, 1217-1227, 1991.

1349 Tréguer, P., Nelson, D.M., Van Bennekom, A.J., Demaster, D.J., Leynaert, A., Quéguiner, B.:
1350 The balance of silica in the world ocean, *Science*, 268, 376-79, 1995.

1351 Tréguer, P., Bowler, C., Moriceau, B., Dutkiewicz, S., Gehlen, M., Aumont, O., Bittner, L.,
1352 Dugdale, R., Finkel, Z., Iudicone, D., Jahn, O., Guidi, L., Lasbleiz, M., Leblanc, K.,
1353 Levy, M., Pondaven, P.: Influence of diatom diversity on the ocean biological carbon
1354 pump, *Nat. Geosci.*, 11, 27–37 (2018).

1355 Tréguer, P., Pondaven P.: Silica control of carbon dioxide, *Nature*, 406, 358–359, 2000.

1356 Tréguer, P.J. & De La Rocha, C.L.: The World Ocean silica cycle, *Ann. Rev. Mar. Sci.*, 5, 477–
1357 501, 2013.

1358 Tréguer, P.J.: The Southern Ocean silica cycle, *Comptes Rendus Geosci.*, 346, 279–286, 2014.

1359 Usbeck, U.: Modeling of marine biogeochemical cycles with an emphasis on vertical particle
1360 fluxes, PhD thesis, University Bremen, 1999.

1361 Von Damm, K.L., Bischoff, J.L. and Rosenbauer, R.J.: Quartz solubility in hydrothermal
1362 seawater: An experimental study and equation describing quartz solubility for up to 0.5
1363 M NaCl solutions, *Am. J. Sci.*, 291, 977-1007, 1991.

- 1364 Wang W., Yang, S., Ran, X., Liu, X.-M., Bataille, C.P., & Su, N.: Response of the Changjiang
1365 (Yangtze River) water chemistry to the impoundment of Three Gorges Dam during
1366 2010–2011, *Chem. Geol.* 487, 1–11, 2018a.
- 1367 Wang, X., Baskaran, M., Su, K., Du, J.: The important role of submarine groundwater discharge
1368 (SGD) to derive nutrient fluxes into river dominated ocean margins – The East China
1369 Sea, *Mar. Chem.*, 204, 121–132, 2018b.
- 1370 Ward, B.A., Dutkiewicz, S., Jahn, O., & Follows, M.J.: A size-structured food-web model for
1371 the global ocean, *Limnol. Oceanogr.*, 57, 1877–1891, 2012.
- 1372 Westberry, T., Behrenfeld, M. J., Siegel, D. A., & Boss, E.: Carbon-based primary productivity
1373 modeling with vertically resolved photoacclimation. *Glob. Biogeochem. Cycles*, 22,
1374 GB2024, 2008.
- 1375 Wheat, C.G., & McManus, J.: The potential role of ridge-flank hydrothermal systems on
1376 oceanic germanium and silicon balances, *Geochim. Cosmochim. Acta*, 69, 2021–2029,
1377 2005.
- 1378 Wheat, C.G., & Mottl, M.J.: Composition of pore and spring waters from Baby Bare: global
1379 implications of geochemical fluxes from a ridge flank hydrothermal system, *Geochim.*
1380 *Cosmochim. Acta.*, 64, 629–642, 2000.
- 1381 Wischmeyer, A.G., De La Rocha, C.L., Maier-Reimer, E., & Wolf-Gladrow, D.A.: Control
1382 mechanisms for the oceanic distribution of Si isotopes, *Glob. Biogeochem. Cycles*, 17,
1383 1083, 2003.
- 1384 Wollast, R., Mackenzie, F.T.: Global biogeochemical cycles and climate, in: *Climate*
1385 *Geosciences: A challenge for science and society in the 21st century*, eds A. Berger,
1386 S.Schneider, & J.C. Duplessy (Dordrecht Springer), 453-473, 1989.
- 1387 Wu, B., Liu, S.M., & Ren, J.L. Dissolution kinetics of biogenic silica and tentative silicon
1388 balance in the Yellow Sea, *Limnol. Oceanogr.*, 62, 1512–152, 2017.
- 1389 Wu, B., Liu, S.M. Dissolution kinetics of biogenic silica and the recalculated silicon balance of
1390 the East China Sea. *Science of The Total Environment*, 2020.
1391 <https://doi.org/10.1016/j.scitotenv.2020.140552>
- 1392 Yang S. L., Xu, K.H., Milliman, J.D., Yang, H.F., & Wu, C.S.: Decline of Yangtze River water
1393 and sediment discharge: Impact from natural and anthropogenic changes, *Sci. Rep.*, 5,
1394 12581, 2015.
- 1395 Zhang, Z., Sun, X., Dai, M., Cao, Z., Fontorbe, G., Conley, D.J.: Impact of human disturbance
1396 on the biogeochemical silicon cycle in a coastal sea revealed by silicon isotopes, *Limnol.*
1397 *Oceanogr.*, 65, 515-528, 2019.

1398 Zhao, B., Yao, P., Bianchi, T., Xu, Y.: Early diagenesis and authigenic mineral formation in
1399 mobile muds of the Changjiang Estuary and adjacent shelf, *J. Mar. Syst.*, 172, 64–74,
1400 2017.
1401

1402 **Table 1. Si inputs, outputs and biological fluxes at world ocean scale**

1403	A-Estimates for Si inputs and outputs	Reference		
1404	Inputs (in Tmol-Si yr ⁻¹)			
1405	F _{R(dSi + aSi)} rivers	8.1 (±2.0)	Frings et al., (2016); Tréguer & De La Rocha (2013)	
1406	F _A aeolian	0.5 (±0.5)	Tréguer & De La Rocha (2013)	
1407	F _W dissolution lithogenic Si	1.9 (±0.7)	Tréguer & De La Rocha (2013)	
1408	F _{GW} submar. groundwater	2.3 (±1.1)	Cho et al. (2018); Rahman et al. (2019); this review	
1409	F _{ISMW} (sub)polar glaciers	0.3 (±0.3)	this review	
1410	F _H hydrothermal	1.7 (±0.8)	this review	
1411	Total inputs estimate	14.8 (±2.6)		
1412				
1413	Outputs (in Tmol-Si yr ⁻¹)			
1414	F _{B(net deposit)} burial	9.2 (±1.6)	this review, Hayes et al. (under review)	
1415	F _{SP} sponges	1.7 (±1.6)	Maldonado et al. (2019)	
1416	F _{RW} reverse weathering	4.7 (±2.3)	Rahman et al. (2016, 2017)	
1417	Total outputs	15.6 (±2.4)		
1418				
1419	B-Comparative estimates of Si fluxes			
1420		Ref. (1) & (2)	this review	Difference (%)
1421	Net inputs (Tmol-Si yr ⁻¹)	9.4 (±4.7)	14.8 (±2.6)	+57 %
1422	Net outputs (Tmol-Si yr ⁻¹)	11.4 (±7.6)	15.6 (±2.4)	+37 %
1423	Gross bSi pelag. prod. (Tmol-Si yr ⁻¹)	240 (±40)	255 (±52)	+06 %
1424	D : P (production: dissolution)	0.56	0.56	
1425				
1426	τ _G residence time (kyears)	12.5 ⁽³⁾	7.7	-38 %
1427	τ _B residence time (kyears)	0.50 ⁽³⁾	0.47	-6 %
1428	τ _G : τ _B	25 ⁽³⁾	16	-34 %
1429	Refs. (1) Nelson et al. (1995) (2) Tréguer & De La Rocha (2013).			
1430	(3) recalculated from our updated dSi inventory value			
1431	See Supplement for detailed definition of flux term (in detailed legend of Fig. 1).			

1432
1433
1434
1435
1436

1437
 1438
 1439
 1440
 1441

Table 2. Biological fluxes ($F_{P_{gross}}$ in $Tmol Si yr^{-1}$)
 Global silica production as determined from numerical models and extrapolated from field measurements of silica production (uncertainties are standard errors)

	World Ocean	Coast	Southern Ocean	Open Ocean
Satellite Productivity models:				
- Chlorophyll level	207 (± 23)	56 (± 18)	60 (± 12)	91 (± 2)
- Ocean Biogeochemical models	276 (± 22)		129 (± 19)	
<i>Average of models</i>	242 (± 49)			
Silica production field studies:				
- Ocean basin ^c	249			
- Domain ^c	285	138	67	80
<i>Average of field studies</i>	267 (± 18)			
Global estimate	255 (± 52)			

1442
 1443
 1444

1445 **Table 3. Twenty-five years of evolution of the estimates for Si inputs, outputs, biological**
 1446 **production, and residence times at world ocean scale**

1447 References : (1) Tréguer et al. (1995), (2) Tréguer & De La Rocha (2013), (3) this review, (4) Nelson et al.
 1448 (1995)

1449 **A-Estimates for Si inputs and outputs fluxes**

1450	References	(1)	(2)	(3)
1451	Inputs (Tmol-Si yr⁻¹)			
1452	F _{R(dSi + aSi)} rivers	5.0 (±1.1)	7.3 (±2.0)	8.1 (±2.0)
1453	F _A aeolian	0.5 (±0.5)	0.5 (±0.5)	0.5 (±0.5)
1454	F _W dissolution lithogenic silica	0.4 (±0.3)	1.9 (±0.7)	1.9 (±0.7)
1455	F _{GW} submar. groundwater	-	0.6 (±0.6)	2.3 (±1.1)
1456	F _{ISMW} (sub)polar glaciers	-	-	0.3 (±0.3)
1457	F _H hydrothermal	0.2 (±0.1)	0.6 (±0.4)	1.7 (±0.8)
1458	Total inputs estimate	6.1 (±2.0)	9.4 (±4.7)	14.8 (±2.6)
1459	Outputs (Tmol-Si yr⁻¹)			
1460	F _{B(net deposit)} burial	7.1 (±1.8)	6.3 (±3.6)	9.2 (±1.6)
1461	F _{SP} sponges	-	3.6 (±3.7)	1.7 (±1.6)
1462	F _{RW} reverse weathering	-	1.5 (±0.5)	4.7 (±2.3)
1463	Total outputs estimate	7.1 (±1.8)	11.4 (±7.6)	15.6 (±2.4)
1464				
1465	B-Estimates for Gross production of biogenic silica (Tmol-Si yr⁻¹)			
1466	References		(4)	(3)
1467	Gross production of biogenic silica		240 (±40)	255 (±52)
1468				
1469	C-Residence time of Si (kyears)			
1470	References	(1)	(2)	(3)
1471	τ _G residence time (geological)	18.3 ⁽⁵⁾	12.5 ⁽⁵⁾	7.7
1472	τ _B residence time (biological)	0.50 ⁽⁵⁾	0.50 ⁽⁵⁾	0.47
1473	τ _G : τ _B	37 ⁽⁵⁾	25 ⁽⁵⁾	16
1474	(5) recalculated from our updated dSi inventory value			
1475				

1476

1477 **Figure 1:** Schematic view of the Si cycle in the modern world ocean (input, output, and
1478 biological Si fluxes), and possible balance (total Si inputs = total Si outputs = 15.6 Tmol-Si yr⁻¹)
1479 in reasonable agreement with the individual range of each flux (F), see Tables 1 and 2. The
1480 white arrows represent fluxes of net sources of silicic acid (dSi) and/or of dissolvable
1481 amorphous silica (aSi) and of dSi recycled fluxes; Orange arrows correspond to sink fluxes of
1482 Si (either as biogenic silica and or as authigenic silica); Green arrows correspond to biological
1483 (pelagic) fluxes. All fluxes are in teramoles of silicon per year (Tmol-Si yr⁻¹). Details in
1484 Supplement section 1.

1485 **Figure 2.** Schematic view of the low temperature processes that control the dissolution of
1486 (either amorphous or crystallized) siliceous minerals in seawater in and to the coastal zone and
1487 in the deep ocean, feeding F_{GW} and F_w . These processes correspond to both low and medium
1488 energy flux dissipated per volume of a given siliceous particle in the coastal zone, in the
1489 continental margins, and in the abysses, and to high-energy flux dissipated in the surf zone.
1490 Details in Supplement section 1.

1491 **Figure 3.** Biogenic silica production measurements in the world ocean. Distribution of
1492 stations in the Longhurst biogeochemical provinces (Longhurst, 2007; Longhurst et al., 1995).
1493 All data are shown in Supplement, section 4 (Annex 1).

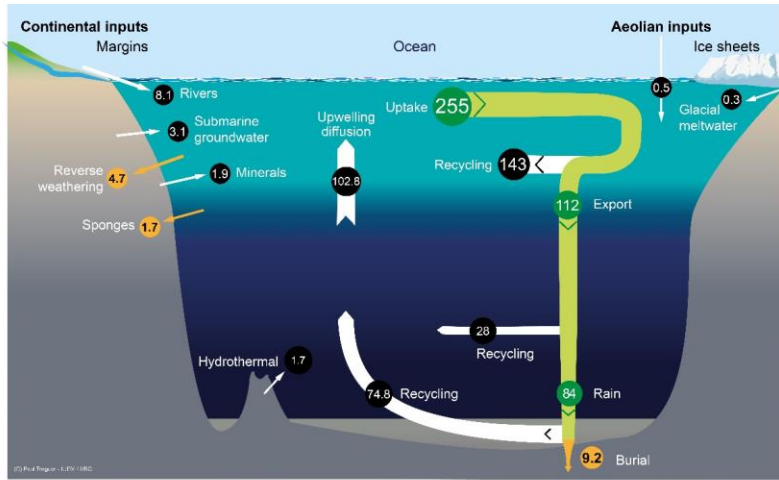
1494 **Figure 4.** Schematic view of the Si cycle in the coastal and continental margin zone (CCMZ),
1495 linked to the rest of the world ocean (« open ocean » zone, including upwelling and polar
1496 zones). In this steady-state scenario, consistent with Fig. 1, total inputs = total outputs = 15.6
1497 Tmol-Si yr⁻¹. This figure illustrates the links between biological, burial and reverse weathering
1498 fluxes. It also shows that the “open ocean” bSi (pelagic) production ($F_{P(gross)} = 222$ Tmol-Si yr⁻¹)
1499 is mostly fueled by dSi inputs from below (92.5 Tmol-Si yr⁻¹), the CCMZ only providing 4.7
1500 Tmol-Si yr⁻¹ to the “open ocean”.

1501

1502

1503 Figure

1(provisional)

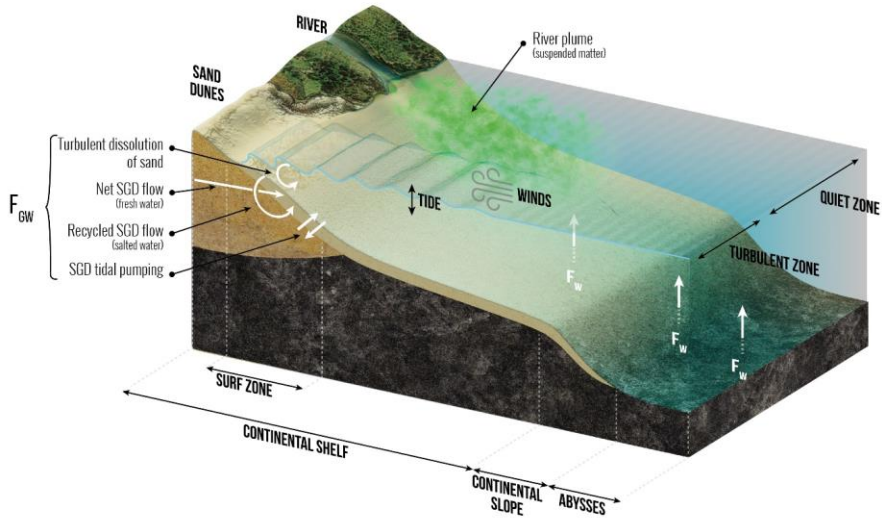


1504

1505

1506

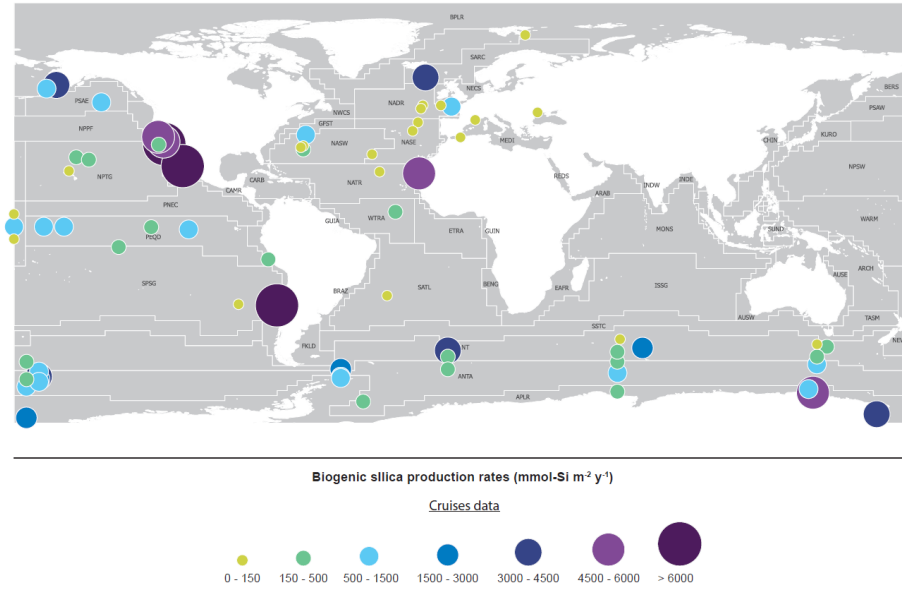
1507 Figure 2



1508

1509

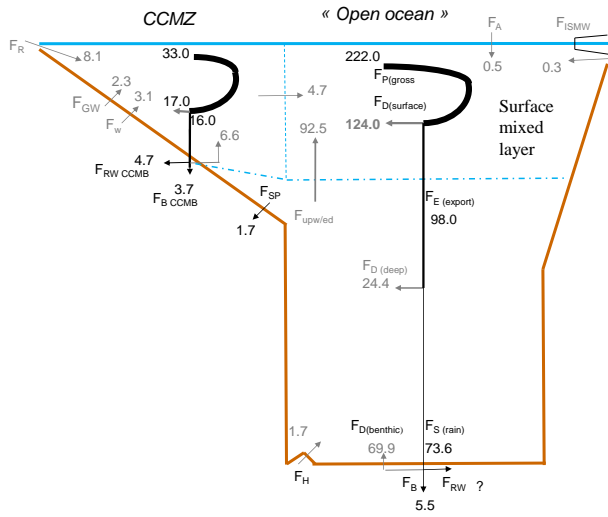
1510 Figure 3



1511

1512

1513 Figure 4



1514

1515